Paleoceanography and Paleoclimatology

RESEARCH ARTICLE
10.1029/2018PA003394

Ocean Circulation in the Toarcian (Early Jurassic): A Key Control on Deoxygenation and Carbon Burial on the European Shelf

Itzel Ruvalcaba Baroni[1], Alexandre Pohl[2], Niels A. G. M. van Helmond[1], Nina M. Papadomanolaki[1], Angela L. Coe[3], Anthony S. Cohen[3], Bas van de Schootbrugge[1], Yannick Donnadieu[2], and Caroline P. Slomp[1]

[1]Department of Earth Sciences, Utrecht University, Utrecht, Netherlands, [2]Aix Marseille Université, CNRS, IRD, Coll France, CEREGE, Aix-en-Provence, France, [3]School of Environment, Earth and Ecosystem Sciences, The Open University, Walton Hall, Milton Keynes, UK

Abstract The Toarcian Oceanic Anoxic Event (T-OAE, ~183 Myr) was a long-lasting episode of ocean deoxygenation during the Early Jurassic. The event is related to a period of global warming and characterized by major perturbations to the hydrological and carbon cycles with high rates of organic matter burial in shelf seas. Ocean circulation during the Toarcian and its influence on marine biogeochemical cycles are still not fully understood. Here we assess the spatial extent of anoxia in the NW Tethys Ocean during the T-OAE, the relationship with ocean circulation and the impact on organic carbon burial, using new and existing sedimentary records from the European Epicontinental Shelf in combination with general circulation model results. We demonstrate that bottom waters on the southwestern part of the shelf were mainly oxic during the T-OAE, while those in the northeastern basins were mostly anoxic or even sulfidic. Results for two ocean-atmosphere models (Fast Ocean-Atmosphere Model and Massachusetts Institute of Technology general circulation model) suggest the presence of a strong clockwise gyre over the European Epicontinental Shelf, which brought oxygenated equatorial waters from the Tethys Ocean to the southern shelf. The northward limb of the gyre was significantly weakened due to the rough bathymetry of the northern shelf, making this relative small region highly sensitive to local ocean stratification. These sluggish ocean dynamics promoted bottom water anoxia and enhanced burial of organic carbon in the northeastern basins, which accounted for 3–5% of the total carbon extracted from the ocean-atmosphere system as recorded by the positive carbon isotope shift.

Key Points:
- The southern European Shelf remained oxygenated during the Toarcian Oceanic Anoxic Event
- Ocean dynamics, notably the Tethyan clockwise gyre, largely controlled bottom water oxygen concentrations on the European Shelf
- Organic carbon burial in the European Shelf likely contributed to the termination of the Toarcian Oceanic Anoxic Event

Supporting Information:
- Supporting Information S1

Correspondence to:
I. Ruvalcaba Baroni,
itzel.ruvalcaba@aces.su.se

Citation:
Ruvalcaba Baroni, I., Pohl, A., van Helmond, N. A. G. M., Papadomanolaki, N. M., Coe, A. L., Cohen, A. S., et al. (2018). Ocean circulation in the Toarcian (Early Jurassic): A key control on deoxygenation and carbon burial on the European shelf. *Paleoceanography and Paleoclimatology*, *33*, 994–1012. https://doi.org/10.1029/2018PA003394

Received 24 APR 2018
Accepted 21 AUG 2018
Accepted article online 25 AUG 2018
Published online 21 SEP 2018

1. Introduction

The Toarcian Oceanic Anoxic Event (T-OAE; ~183 Myr) is one of several long-lasting episodes (>100 kyr) of ocean deoxygenation during the Mesozoic (e.g., Jenkyns, 2010). The T-OAE can be recognized in sedimentary rocks deposited during the Early Jurassic by a major negative carbon isotope excursion in both terrestrial and marine organic matter. It is associated with global warming superimposed on an already warm climate (e.g., Hesselbo et al., 2000; Kemp et al., 2005). Plausible causes for warming during the T-OAE are the injection of massive amounts of CO_2 into the atmosphere due to the emplacement of the Karoo-Ferrar large igneous province and large-scale release of thermogenic methane (Cohen et al., 2004; Hermoso et al., 2009; Hesselbo et al., 2000; Kemp et al., 2005). The carbon isotope shift during the event has been attributed to the dissociation of methane hydrates (e.g., Beerling & Berner, 2002; Cohen et al., 2007; Kemp et al., 2005), magmatic intrusions into organic-rich sediments (McElwain et al., 2005), and volcanic activity (e.g., Suan, Mattioli, et al., 2008; Svensen et al., 2007). The T-OAE is characterized by global changes in climate and biogeochemical cycling (Cohen et al., 2004).

Sedimentary rock records indicate that parts of the European Epicontinental Shelf (EES; Figure 1) were particularly susceptible to deposition of organic-rich sediments, likely reflecting bottom water anoxia during the T-OAE (Jenkyns, 1985; McArthur et al., 2008). This holds in particular for the northern basins of the EES, where there are several lines of evidence for persistent anoxic and sulfidic bottom waters (i.e., euxinia) developing during the event, only interrupted by occasional periods of brief reoxygenation. After the termination of the T-OAE, the area with marine anoxia/euxinia contracted (e.g., Dickson et al., 2017; Frimmel et al., 2004; McArthur et al., 2008; Pearce et al., 2008; Röhl et al., 2001; Them et al., 2018; Thibault et al., 2018).

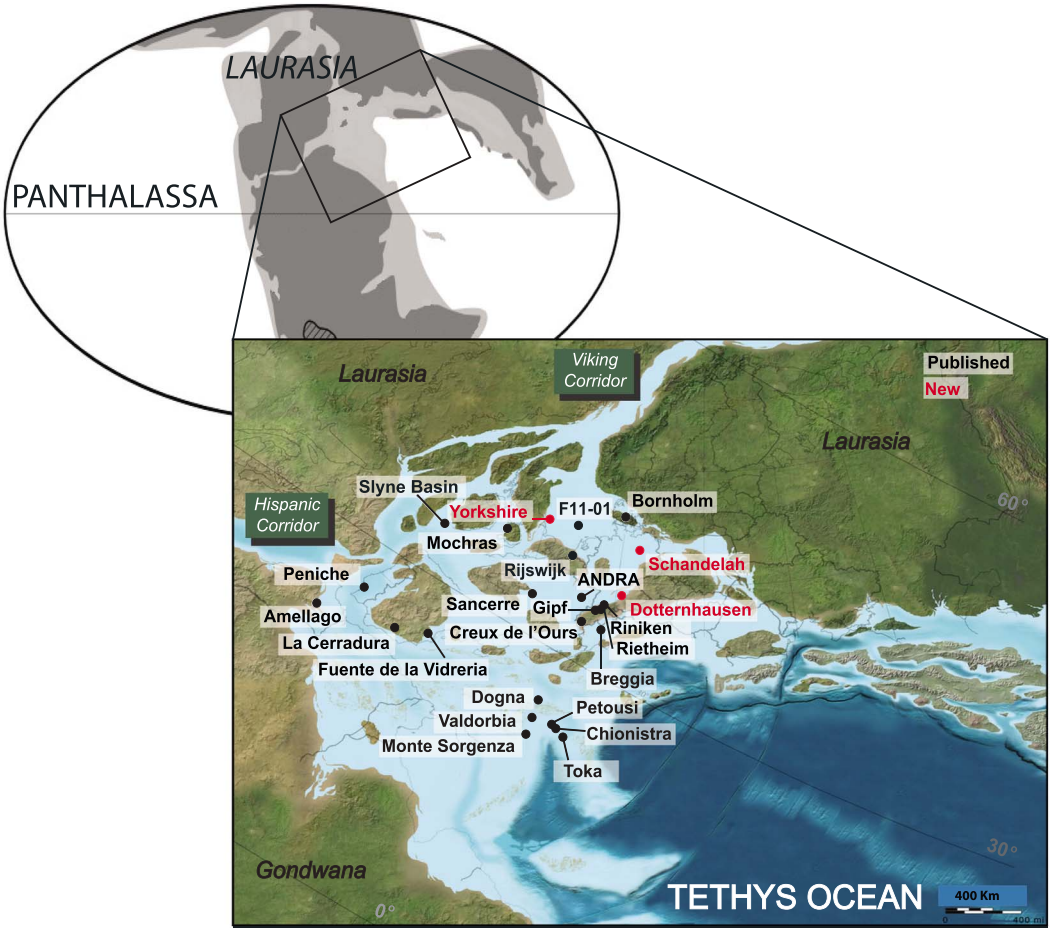

Figure 1. Toarcian paleogeographical reconstruction of the Earth and the NW Tethys Ocean with adjacent shallow region. This shallow region is here referred to as the European Epicontinental Shelf. Note the lack of sampling sites in the open Tethys Ocean, the Viking and Hispanic corridors, and the southern European Epicontinental Shelf. Locations of sites with new (red) and published (black) data compiled for this study are indicated. Thin black lines represent the equator and the 30°N parallel. The global map is modified from Them et al. (2017) and regional paleogeography is modified from reconstructions by Ron Blakey, Deep Time Maps^{TM}, https://deeptimemaps.com/gmedia-album/.

Although the EES accounted for only a small proportion of the global ocean during the Toarcian, the amount of organic matter buried in the sediment during the T-OAE could have been sufficient to impact atmospheric CO_2 concentrations, thereby providing a negative feedback on the warming. The potential of this mechanism is illustrated by the recent finding that organic carbon burial in one single freshwater lake was of sufficient magnitude to contribute between 1.3% and 2.2% of the global drawdown of atmospheric CO_2 required to recover from the negative isotope shift during the Toarcian (Xu et al., 2017).

Despite the apparent global-scale importance of the biogeochemical changes in the EES and other shallow shelf seas during the Toarcian, the exact spatial extent of the anoxia and the oceanographic conditions leading to the organic matter burial are not well understood. This particularly holds for the ocean circulation in the Tethyan region. An example is the flow through the Viking Corridor (Figure 1), which has both been suggested to be southward from the Arctic (Bjerrum et al., 2001), with the flow dominating the entire shelf (Dera et al., 2009) and northward from the Tethys Ocean to the Arctic (Korte et al., 2015). Various studies suggest a role of a warm surface current flowing from the Tethys Ocean to the shelf, mainly based on geological records (Dera et al., 2015; Krencker et al., 2015; Röhl et al., 2001). Modeling studies for the Early Jurassic mainly focus on atmosphere dynamics (e.g., Chandler et al., 1992; Sellwood & Valdes, 2008; Valdes et al., 1995) and differ in modeled seasonal contrast, global air surface temperatures, and the magnitude of polar ice cap formation. The only study using an ocean-atmosphere model to assess the response of ocean dynamics under different atmospheric CO_2 levels during the Toarcian is that of Dera and Donnadieu (2012). They concluded

that during the Toarcian, the strength of the global ocean circulation progressively decreased and that frequent discharges of brackish Arctic surface waters may have flowed through the Viking Corridor into the EES. Based on osmium isotopes (Cohen et al., 2004; Percival et al., 2016; Them et al., 2017) and kaolinite/illite ratios (Xu et al., 2018), enhanced weathering due to an increased hydrological cycle has been suggested to have dominated the T-OAE interval.

Here we first describe the spatial extent of anoxia in the EES during the T-OAE based on existing and newly generated records of redox-sensitive elements from sites in the Cleveland and German basins in the northeast of the EES. We also estimate rates of organic carbon burial based on the sedimentary rock records. Two ocean-atmosphere general circulation models—the Fast Ocean-Atmosphere Model (FOAM; Jacob, 1997) and the Massachusetts Institute of Technology general circulation model (MITgcm; Adcroft et al., 2004)—are used to assess the potential role of ocean circulation in explaining the spatial trends in biogeochemical conditions in the EES. We show that the bathymetry of the EES and the clockwise flow of water played a critical role in the development of anoxia on the shelf and the burial of organic carbon.

2. Background

2.1. Study Area

During the Early Jurassic, relative sea level rise led to the formation of various interconnected epicontinental seas, in what is now western Europe (Figure 1). This region, which we refer to as the EES, was connected to the open Tethys Ocean (Ziegler, 1988, 1990) and is characterized by numerous islands in the north. The exact bathymetry of the EES is uncertain (e.g., Baudin et al., 1990; Golonka & Ford, 2000), but there is evidence from the geological record for both shallow areas (<300 m; Farrow, 1966; Trabucho-Alexandre et al., 2012) and deeper basins (~2,500 m; Röhl et al., 2001; Tissot et al., 1971). The EES was located near the Tropic of Cancer and was about 2000–3000 km wide and 4,000–6,000 km long (Ziegler, 1988). It accounted for about 3% of the global ocean surface. Important seaways, the Hispanic and Viking corridors, connected the EES with the Panthalassa and the Arctic Oceans. Their precise opening times and depths remain uncertain for T-OAE, but paleontological evidence suggests connections that allowed the migration of marine species between oceans (e.g., Aberhan, 2001, 2002; Arias, 2006; Caswell & Coe, 2014; Mattioli et al., 2008; Nikitenko, 2008).

The EES saw various episodes of deposition of organic-rich mudrocks. The lower Toarcian succession is a prime example since it contains the most pronounced carbon isotope excursion—that is, T-OAE (Jenkyns et al., 2002). The Toarcian Stage presents geological evidence of different Milankovitch frequencies (precession, obliquity, and eccentricity). However, which of the orbital parameters controlled the sediment cycles during the T-OAE remains unclear (Boulila et al., 2014; Huang & Hesselbo, 2014; Kemp et al., 2005, 2011; Ruebsam et al., 2014, Sha et al., 2015). The onset of organic-rich mudrock deposition may have been diachronous in the EES during the Toarcian (Wignall et al., 2005). However, the principal level of organic-rich mudrock can generally be assigned to the lower to middle *Harpoceras exaratum* Subzone (in terms of ammonite zonation). Geological evidence suggests that primary productivity and burial rates of organic matter increased over the entire EES during the T-OAE (Bodin et al., 2010; Rodríguez-Tovar & Reolid, 2013; Suan, Mattioli, et al., 2008). Monsoon winds are likely to have dominated the north-eastern Tethys Ocean (Parrish & Curtis, 1982), which would have favored precipitation over evaporation across the EES leading to enhanced river discharge and terrestrial nutrient inputs (Röhl et al., 2001), especially along the western Laurasian coast (Chandler et al., 1992; Valdes et al., 1995). These conditions could have been responsible for the deoxygenation that developed in bottom waters. Short-lived oxygenation events are likely to have occurred during the T-OAE, which were possibly linked to a switch in wind patterns that would have favored dry conditions (Röhl et al., 2001). Geological evidence for enhanced continental runoff has been found in the EES (e.g., Fantasia et al., 2018; Hesselbo et al., 2007). The highest total organic carbon (TOC) contents are mainly found along the northeastern side of the EES (Jenkyns, 1988; Kemp et al., 2011). Most of the organic matter preserved in T-OAE sediments in the EES is of marine origin (e.g., Frimmel et al., 2004; Mailliot et al., 2009; Montero-Serrano et al., 2015; Trabucho-Alexandre et al., 2012).

2.2. Redox Proxies

Various elemental ratio and elemental concentration geochemical proxies are available to reconstruct local and regional bottom water oxygen conditions from sedimentary rock records (e.g., Calvert & Pedersen, 1996; Tribovillard et al., 2006). Here we briefly describe the redox proxies used in this study, including the mechanisms that are thought to be responsible for the observed signals.

Elevated ratios of TOC to total phosphorus (TOC/P) reflect enhanced regeneration of P relative to carbon in sediments overlain by low-oxygen waters. The elevated ratios are thought to be the combined result of less retention of P by microorganisms and less retention in minerals in the sediment (e.g., as Fe oxide bound P and apatite; Algeo & Ingall, 2007; Ingall et al., 1993; Slomp et al., 2002). Ratios of iron over aluminum (Fe/Al) above crustal averages (0.5 wt%/wt%) are typically associated with anoxic and sulfidic basins, where Fe becomes enriched through effective trapping of any incoming Fe from shallower areas (Lyons & Severmann, 2006; Owens et al., 2012). Because input from these shallower areas can be enhanced under anoxic but not sulfidic conditions, Fe/Al can also indicate how widespread anoxia is in a region (e.g., Eckert et al., 2013; Lenz et al., 2015; Raiswell & Anderson, 2005). Molybdenum (Mo) is conservative in oxic waters but is fixed in sediments in the presence of free hydrogen sulfide through conversion of molybdate to particle reactive thiomolybdate (Helz et al., 1996). While near crustal values of Mo (1–2 ppm) indicate oxic bottom waters, enrichments of <25 ppm typically reflect the presence of sulfide in pore waters only and values above 60 to 100 ppm are often used as an indicator for euxinic bottom waters (Lyons et al., 2009; Scott & Lyons, 2012). However, the removal of Mo through sediments in low-oxygen waters can be faster than the resupply of Mo by renewal of the water mass, which would lower the Mo concentrations in sediments of restricted basins (Algeo & Lyons, 2006). Sediments in euxinic basins are often enriched in sulfur (S), copper (Cu), and vanadium (V). The S is mostly in the form of pyrite (Lyons & Berner, 1992), with formation of pyrite being limited by the input of Fe (Berner, 1970). While Cu is typically enriched in pyrite in S-rich sediments, V generally precipitates in authigenic mineral phases (e.g., Algeo & Maynard, 2004; Hastings et al., 1996; Tribovillard et al., 2006). Enrichments of manganese (Mn) are common in environments with variations in bottom water redox conditions, which allow Mn oxides to be converted to Mn carbonates. In sediments permanently overlain by anoxic bottom waters, sediment concentrations of Mn are typically low because the Mn oxides are not preserved and are not converted to other Mn mineral forms. Consequently, the Mn is not buried (e.g., Calvert & Pedersen, 1996; Lenz et al., 2015).

3. Methods

3.1. Geological Observations

Sedimentary records of TOC, TOC/P, Fe/Al, Mo, Mn, S, V, and Cu from Toarcian successions at Yorkshire (UK), Schandelah (Northern Germany), and Dotternhausen (Southern Germany) were generated and combined with existing TOC and redox proxy data for the northwestern Tethyan region during T-OAE. All sites from which geochemical records were used in this study are shown in Figure 1. Relevant average geochemical data for the carbon isotope excursion at each site and references (e.g., French et al., 2014; Jenkyns et al., 2001; Lu et al., 2010; Silva et al., 2017; Van Breugel et al., 2006) are given in the supporting information (Table S1). The table also includes a compilation of the evidence for high/low primary productivity, the degree of oxygenation, and photic zone euxinia deduced mainly from palynology and from the presence of specific organic compounds, such as isorenieratane and methyl isobutyl maleimides. Below, we briefly describe the geological setting and sampling of the Yorkshire, Schandelah, and Dotternhausen sites, which all represent shallow depositional environments, with paleodepths not greater than 200 m during the T-OAE.

3.1.1. Yorkshire (UK)

The Yorkshire succession was deposited in the Cleveland Basin in the northern EES. The samples were collected from a composite of the Toarcian exposures at Saltwick Bay, Port Mulgrave, and Hawsker Bottoms along the coast of North Yorkshire in the UK. The T-OAE in Yorkshire is characterized by unbioturbated, laminated marine organic-rich mudrocks with discrete levels of calcite concretions and spans the upper *tenuicostatum* and lower *falciferum* Ammonite zones (Howarth, 1992; Kemp et al., 2005). These exceptionally well preserved sedimentary rocks provide a complete record of the T-OAE. The biostratigraphy and lithostratigraphy presented here are from Howarth (1992). The TOC, P, Fe/Al, Mn, Mo, S, V, and Cu data from this location used in this study are from Harding (2004). The carbon isotope record, which was completed on exactly the same samples, was published in Cohen et al. (2004). The samples were collected at least every 50 cm and at a spacing of up to 1 cm from the T-OAE interval. High-resolution carbon isotope, TOC, and S data are also available in Kemp et al. (2005) and Kemp et al. (2011). Molybdenum concentration determined by isotope dilution on aliquots of many of the same samples used in this study are presented in Pearce et al. (2008).

3.1.2. Schandelah (Northern Germany)

The Schandelah site was located in the northern German Basin during the Early Jurassic. The core drilled at Schandelah mainly consists of laminated, organic-rich gray and black shales (van Eldijk et al., 2018). The $\delta^{13}C_{org}$

Table 1
Summary of the Experiments Used in This Study, Where the Orbital Parameters (Eccentricity, Obliquity, and Perihelion), the Paleogeography, and the Paleodepths of the EES Are Varied to Test Their Influence on Ocean Circulation

				Orbital configuration		
Model	Experiment	Paleoreconstruction	Seasonality	Eccent.	Obli.	Perihelion
FOAM	PR1	Dera and Donnadieu (2012)	Minimum	0	22	—
	$PR1_{InsolStrong}$	Dera and Donnadieu (2012)	Strong	0.05	24.5	June
	$PR1_{InsolWeak}$	Dera and Donnadieu (2012)	Weak	0.05	24.5	December
	$PR1_{closed}$	Dera and Donnadieu (2012) and closed Hispanic Corridor	Weak	0.05	24.5	December
	PR2	Golonka and Ford (2000)	Minimum	0	22	—
	$PR2_{shallow}$	Golonka and Ford (2000) and shallow continental shelves in the EES (up to 30 m)	Weak	0.05	24.5	December
MITgcm	$PR1_{MIT}$	Dera and Donnadieu (2012)	Minimum	0	23.45	—
	$PR2_{MIT}$	Golonka and Ford (2000)	Minimum	0	23.45	—

Note. All our experiments assume warm initial seawater temperatures. Experiments performed with Fast Ocean-Atmosphere Model (FOAM) assume a pCO_2 of 1,120 ppm and a solar constant of 1,343 W/m^2, while those performed with Massachusetts Institute of Technology general circulation model (MITgcm) assume a pCO_2 of 326 ppm and a solar constant of 1,380 W/m^2 (for more details, see supporting information section S2.1). The seasonal contrast in the Northern Hemisphere (seasonality) for each experiment is indicated. Note that all scenarios presented in Dera and Donnadieu (2012) assume a cold ocean as initial condition, as well as the modern distribution of insolation (eccentricity = 0.017 and obliquity = 23.43) with a solar constant of 1,344.07 W/m^2. EES = European Epicontinental Shelf.

and detailed stratigraphy are published in van de Schootbrugge et al. (2018). The T-OAE interval is identified based on selected palynological data of the onset, combined with the negative excursion of the $\delta^{13}C_{org}$ and the TOC content (supporting information section S1.1 and Figure S1.1; Cochlan et al., 1991; Falcón et al., 2004; van de Schootbrugge et al., 2013). The organic-rich mudrocks related to the negative carbon isotope excursion are present within the *tenuicostatum* and the lower *falciferum* Ammonite zones (Brumsack, 1991; van de Schootbrugge et al., 2013). Here the *tenuicostatum* Zone is represented in a 5-cm interval. The sampling resolution was 10 cm with a resolution of 5 cm in parts of the T-OAE interval.

3.1.3. Dotternhausen (Southern Germany)

The Dotternhausen site was located in the southern German Basin during the Early Jurassic (e.g., Röhl et al., 2001). The paleodepth was likely a few tens of meters (Röhl & Schmid-Röhl, 2005). The organic-rich sedimentary rocks consist of a succession of marls and bituminous clays with a few interbedded carbonate-rich levels (Röhl et al., 2001). The T-OAE, identified by a negative shift in $\delta^{13}C_{org}$ of approximately 5‰, is located within the middle *semicelatum* and *elegans* Ammonite subzones, between approximately 2 and 5.5 m (Schouten et al., 2000). The lithology and (bio)stratigraphy presented here are from Riegraf et al. (1984), and the $\delta^{13}C_{org}$ record is from Schouten et al. (2000). The TOC, P, Fe/Al, Mo, Mn, S, V, and Cu data are from Harding (2004) from samples collected every 5 to 20 cm.

3.1.4. TOC and Elemental Composition

Sedimentary samples from Yorkshire and Dotternhausen were crushed and homogenized in an agate mortar. TOC and S were determined using the Leco CNS-2000 Elemental Analyser at the Open University, UK. The TOC was calculated as the difference between 0.2 g of sample analyzed for bulk carbon content and the remaining carbon content from 0.3 g of sample that was ashed in a furnace at 450 °C to oxidize all the organic carbon. Other elements (P, Fe, Al, Mn, Mo, V, and Cu) were determined from glass beads and pressed pellets using the ARL 8420+ dual goniometer wavelength dispersive X-ray florescence spectrometer at the Open University, UK. Sediment samples from Schandelah were freeze dried, powdered, and homogenized using an agate mortar and pestle. To determine the organic carbon content, about 0.3 g of powdered sample was decalcified using 1 M HCl. Subsequently, carbon was quantified in the decalcified residue by a Fisons Instruments CNS NA 1500 analyzer, and the TOC content of the original sampled was calculated after correcting for the weight loss (Van Santvoort et al., 2002). To measure the total elemental composition, approximately 125 mg of powdered sample was treated with 2.5 ml of mixed acid ($HClO_4$:HNO_3; 3:2) and 2.5 ml 40% HF, followed by evaporation of the acids and redissolution of the residue in 25 ml 4.5% HNO_3. The solutions were then analyzed for P, Fe, Al, Mo, Mn, S, V, and Cu with a Coupled Plasma-Optical Emission Spectrometry (SPECTRO ARCOS). The accuracy was between 95% and 105%, and the relative errors were < 5% for all reported elements.

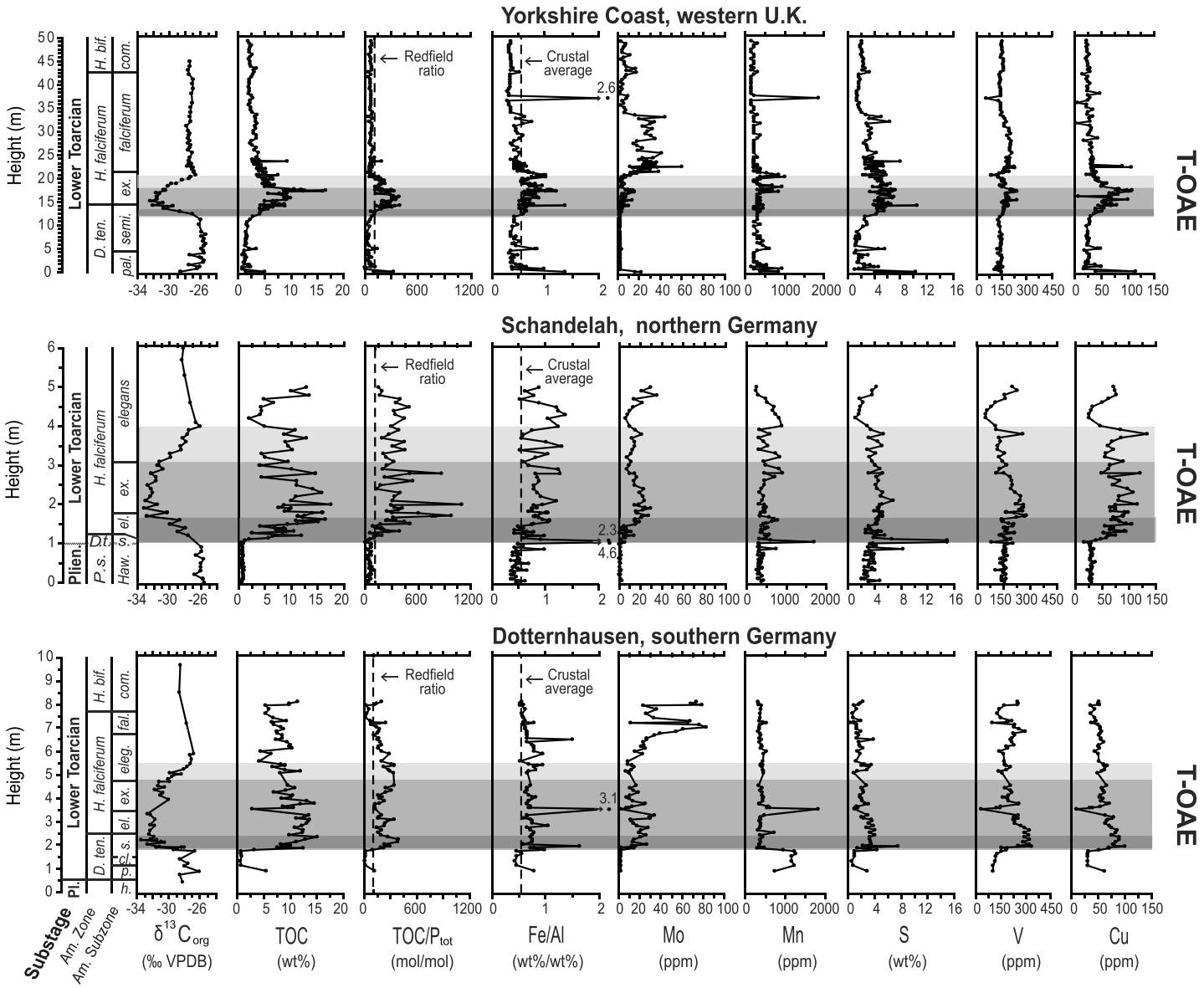

Figure 2. Lithology; chemostratigraphy ($\delta^{13}C_{org}$ and TOC); redox-sensitive elements (TOC/P, Fe/Al, Mo, Mn, V, and Cu); and S at Yorkshire, Schandelah, and Dotternhausen. Gray shades highlight the initiation, the main interval, and the termination of T-OAE (after Cohen et al., 2004). Carbon isotopes at Yorkshire, Schandelah, and Dotternhausen are from Cohen et al. (2004), van de Schootbrugge et al. (2018), and Schouten et al. (2000), respectively. For other references see text. VPDB = Vienna PeeDee Belemnite; T-OAE = Toarcian Oceanic Anoxic Event; TOC/P = total organic carbon to total phosphorus.

3.2. Models

We use the fully coupled FOAM and MITgcm to assess the water circulation in the EES. Both FOAM and MITgcm resolve global circulation, sea ice, land surface, and river transport, with an ocean medium resolution grid of 1.4° × 2.8° and 1.85° × 1.85°, respectively. While FOAM is specifically designed for long-term simulations (Jacob, 1997), MITgcm is computationally more expensive. However, MITgcm provides a more robust representation of the ocean dynamics and mixing processes than FOAM (Gent & Mcwilliams, 1990; Large et al., 1994). Results of both models for the modern ocean compare well with those of higher-resolution climate models (Jacob et al., 2001; Marshall et al., 1998; Tobis et al., 1997). Here we use FOAM to explore a wide range of boundary conditions for the T-OAE and MITgcm to determine to what extent our results are model dependent. Our baseline scenario for the T-OAE (PR1) is based on that of Dera and Donnadieu (2012), which includes a pCO_2 that is 4 times the preindustrial level (i.e., 1,120 ppm). The present-day orbit and insolation used in Dera and Donnadieu (2012) were replaced by an orbital configuration imposing a minimal seasonal

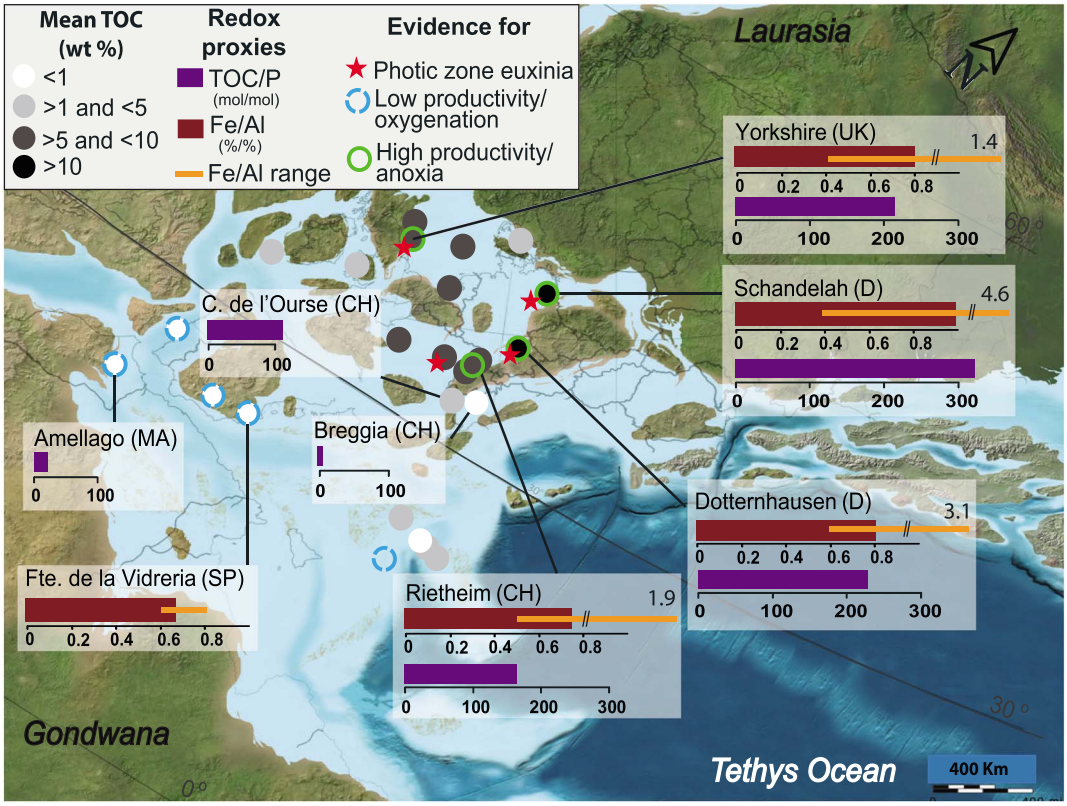

Figure 3. Summary of new and existing redox-sensitive elements from the European Epicontinental Shelf during T-OAE. The map shows the spatial distribution of the averaged TOC, TOC/P, Fe, and Mn within T-OAE and for sites where data was available. The range of Fe/Al across T-OAE (i.e., minimum and maximum values) are indicated (orange bars). Note that the small parallel lines indicate that maximum values exceed the *x* axis limit. Locations that show evidence for euxinic, anoxic, or oxygenated conditions are indicated. Evidence for low/high primary productivity inferred from different studies is also shown. See text and Table S1 for details and references. T-OAE = Toarcian Oceanic Anoxic Event; TOC/P = total organic carbon to total phosphorus.

contrast in the Northern Hemisphere and a smaller solar constant, respectively (Table 1). In the experiments of Dera and Donnadieu (2012), the initial ocean temperatures were set to modern values. This initial cold ocean favors surface warming and stratification. We therefore use warm initial temperatures to ensure a rapid deep-ocean equilibrium. The Toarcian paleogeography (van de Schootbrugge et al., 2005) and orbital forcing parameters are poorly constrained with estimates for the T-OAE interval (i.e., the negative CIE) ranging from approximately 300 to 900 kyr (e.g., Boulila et al., 2014; Huang & Hesselbo, 2014; Kemp et al., 2005, 2011; Ruebsam et al., 2014; Sha et al., 2015; Suan, Pittet, et al., 2008). Therefore, we conduct five additional FOAM experiments with different orbital forcing parameters, paleogeography, and bathymetry settings (Table 1 and Figure S2.1). For the orbital forcing parameters in particular, we considered two end-members characterized by a seasonality that is either extremely weak or extremely strong in the northern midlatitudes ($PR1_{InsolWeak}$ and $PR1_{InsolStrong}$ respectively; see Table 1). In this study, we use two different paleogeographic reconstructions, based on those of Golonka and Ford (2000) and Dera and Donnadieu (2012), which mainly differ in the latitudinal position of the main continental blocks and the position, number, and size of emerged landmasses in the EES region. The latitudinal position of the EES in the paleogeographic reconstruction of Golonka and Ford (2000) is more in agreement with the geological database than that of Dera and Donnadieu (2012). One MITgcm model run is conducted for each of the paleogeographic reconstructions (Table 1). In the MITgcm experiments, greenhouse gas concentrations cannot be changed and the simulation of warm climatic states was achieved by increasing the solar constant, following the methodology used in Ferreira et al. (2011) and Pohl et al. (2017). The resulting global climatic state is comparable to the one simulated with FOAM (pCO_2 of 1,120 ppm). Model details are further described in supporting information S2 (e.g., Forget et al., 2015; Gent & Mcwilliams, 1990; Gough, 1981; Jacob, 1997; Pacanowski & Philander, 1981).

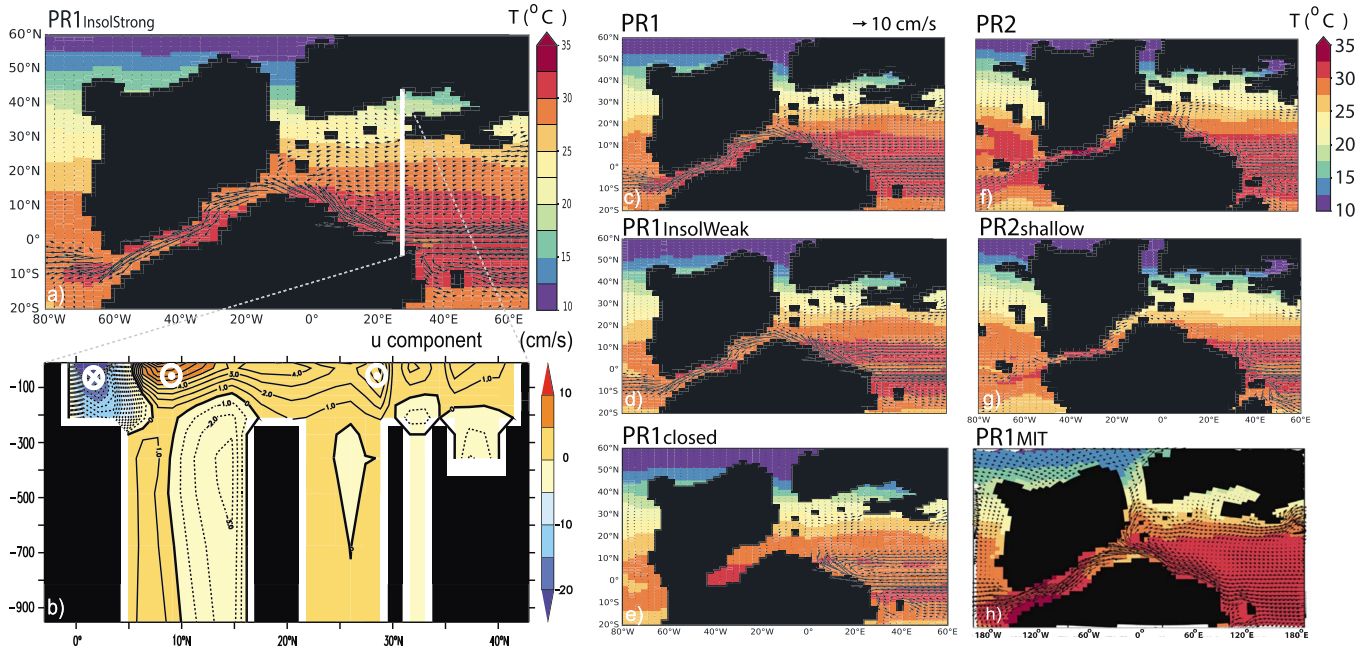

Figure 4. Ocean dynamics in the Tethyan region for scenarios with contrasting orbital forcing, bathymetry, and two different paleogeographic reconstructions (PR1 is based on Dera & Donnadieu, 2012, and PR2 on Golonka & Ford, 2000). In (a) and (b) results are shown for the scenario with a strong insolation in the Northern Hemisphere ($PR1_{InsolStrong}$). Panel (a) shows the surface ocean currents (vectors) and sea surface temperatures (color) averaged over the first 100 m. Panel (b) shows the E-W velocity component (*u*) flowing in and out of the EES through a transect (at 27°E). The circles indicate the main direction of the flow dominating the first 300 m, where ⊗ refers to westward flow and ⊙ to eastward flow. The transect is indicated by the white line in (a). Other results are for the surface ocean currents (vectors) and sea surface temperatures (color) for (c) the base line scenario (PR1), (d) the scenario with a weak insolation in the northern Hemisphere ($PR1_{InsolWeak}$), (e) the scenario with a closed Hispanic Corridor ($PR1_{closed}$), (f) the scenario with an updated paleogeographic reconstruction (PR2), (g) the scenario with a shallow EES (up to 30 m) and an updated paleogeographic reconstruction, and (h) the scenario performed with Massachusetts Institute of Technology (MIT) general circulation model ($PR1_{MIT}$). For more details on each scenario, see Table 1. EES = European Epicontinental Shelf.

3.3. Estimation of the Organic Carbon Burial

The TOC (in gigatons) stored in EES sediments during the T-OAE was calculated following the equation used in Xu et al. (2017): $M = A \times h \times \rho \times TOC$, where *M* is the TOC for a chosen area, *A* is the area, *h* is the averaged thickness of *A*, and ρ is the sediment bulk density (here assumed to be 2.5 g/cm^3; Wei et al., 2014). The TOC is estimated based on the TOC of each site averaged over the T-OAE interval and then averaged over the total number of sites included in the respective area. We use the model paleogeography and bathymetry to calculate the area, which is chosen to include sites with similar TOC content that are located within similar basins. The thickness (*h*) is then estimated based on the averaged thickness of all T-OAE deposits within the given area *A*. Values of *h* and *A* used in this study are given in supporting information S1 (Table S1 and Figure S1.2).

4. Results

4.1. Geochemical Data From the NE Basins

Sedimentary records from Yorkshire, Schandelah, and Dotternhausen show strong similarities despite being located in different basins of the EES (Figure 2). At all three sites, the negative carbon isotope excursion of ~5‰ to 7‰ in organic carbon that characterizes the event coincides with the deposition of highly organic rich sediments, with TOC contents up to ~20 wt%. However, the TOC contents are higher at Schandelah and Dotternhausen than at Yorkshire. At all sites, we find low values of TOC/P, Fe/Al, Mo, V, S, and Cu prior to the event and increased values characterized by a large temporal variability during the T-OAE. Molar TOC/P ratios are typically above the Redfield ratio (i.e., 106) during the event, with maximum values ranging from ~400 at Yorkshire and Dotternhausen to ~1,200 at Schandelah. Fe/Al ratios are typically higher than the crustal average of 0.5 wt%/wt% and mostly below 1 wt%/wt% during the event. Concentrations of Mo increase at all sites to values between ~10 and 30 ppm. Manganese contents are typically low but show quite some variation, with maxima in and/or at the end of the T-OAE at all sites. Sulfur, V, and Cu are enriched in the T-OAE sedimentary rocks at all sites.

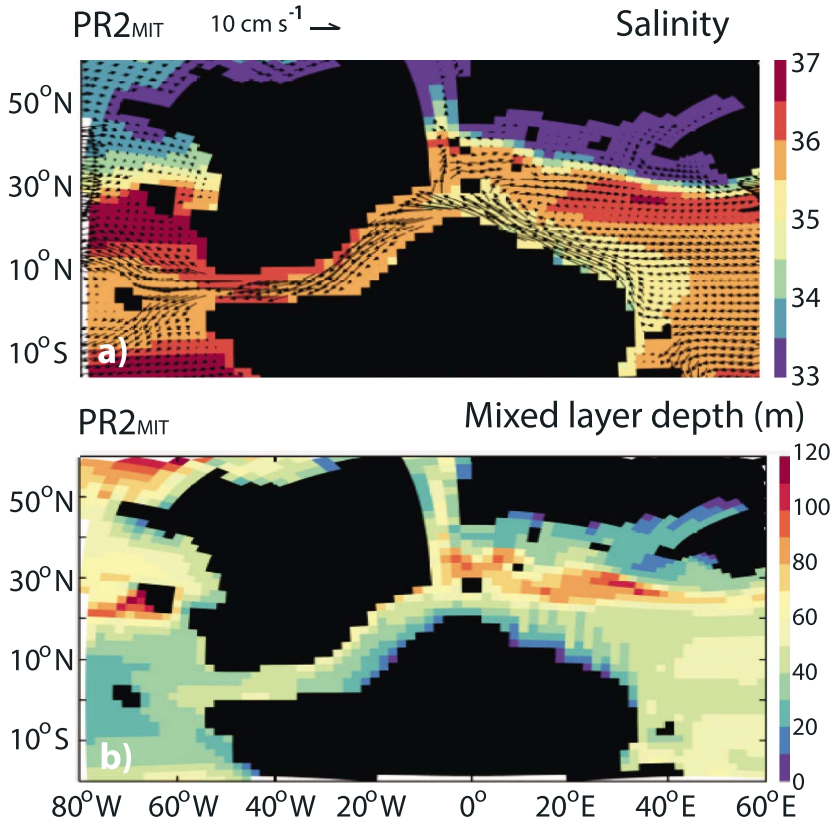

Figure 5. Ocean circulation, salinity, and mixed layer depth simulated in the European Epicontinental Shelf by experiment $PR2_{MIT}$. (a) Surface ocean currents (vectors) and mean annual ocean salinity (color) averaged over the first 100 m of the water column. (b) Mean annual mixed layer depth. Results of Massachusetts Institute of Technology (MIT) general circulation model are shown because the latter model provides a more robust representation of mixing processes and thus mixed layer depth than Fast Ocean-Atmosphere Model.

After the T-OAE, trends at the three sites diverge. While at the Yorkshire site, TOC/P and Fe/Al decrease to background values, relatively high values are still observed at the other two sites. Concentrations of TOC remain high while Mo concentrations further increase at all sites after the T-OAE. At Schandelah, this increase is preceded by a minimum in Mo, which coincides with a minimum in TOC, S, V, and Cu and a maximum in Mn. The Yorkshire record ranges from the *tenuicostatum* Zone to the lower *bifrons* Zone and contains the most expanded *falciferum* Zone. At this site, differences between the lower (~21–34 m) and upper (~34–42.2 m) *falciferum* Subzone can be distinguished. For example, during the lower *falciferum* Subzone, TOC decreases with increasing Mo concentrations. In contrast, Mo concentrations decrease while TOC remains relatively low during the upper *falciferum* Subzone (Pearce et al., 2008).

4.2. Spatial Trends in Organic Carbon and Redox Proxies During the T-OAE

Our data compilation of TOC and redox proxy data for the EES during the T-OAE reveals two major contrasting depositional settings (Figure 3). Whereas organic carbon-rich sediments (>1 wt% TOC) were deposited in the northern EES (above 30°N), relatively organic-lean sediments (<1 wt% TOC) are found in the south. The highest TOC contents (>5 wt%) are observed in the northwestern basins (Yorkshire, Schandelah, Dotternhausen, and Rietheim). These sedimentary rocks are also characterized by high molar TOC/P ratios (>150), high Fe/Al, and low Mn/Al. Such a geochemical signature is typical for sediments overlain by low-oxygen bottom waters (Algeo & Maynard, 2004; Mort et al., 2010; Sulu-Gambari et al., 2017). Sediments at these sites also show evidence for a high primary productivity and photic zone euxinia as deduced from micropaleontological records, Rock-Eval pyrolysis and biomarker analysis (supporting information Table S1).

In the southern EES, in contrast, low TOC/P (<106) and low Fe and Mo suggest oxic (at most suboxic) conditions during T-OAE. However, the absence of benthic fauna, weak bioturbation, occurrence of finely laminated sediments (Suan, Mattioli, et al., 2008), and the occasional presence of pyrite fromboids (Reolid et al., 2014)

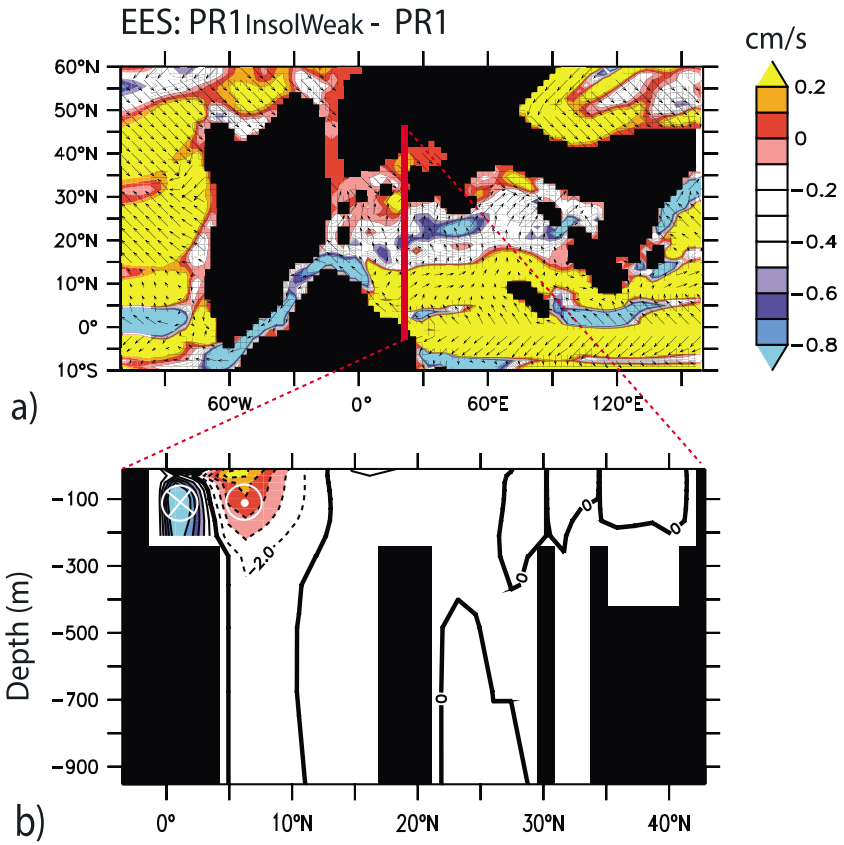

Figure 6. Difference in ocean dynamics in the NE Tethys region, including the EES, between a scenario with reduced and minimum seasonal contrast in the Northern Hemisphere ($PR1_{InsolWeak}$ − PR1). (a) The direction of mean annual surface ocean currents (vectors) averaged over the first 100 m of the water column and the difference in magnitude (color) between $PR1_{InsolWeak}$ and PR1. (b) Difference in the E-W velocity component (*u*) between $PR1_{InsolWeak}$ and PR1 flowing through a transect dividing the EES and the open Tethys Ocean. Main direction of the flow dominating the first 300 m are brought forward by the circles, where ⊗ indicates a westward flow and ⊙ an eastward flow. The corresponding transect is indicated in (a). White color indicates zones of no or little differences. EES = European Epicontinental Shelf.

suggest short episodes of reducing conditions in bottom waters at Peniche and La Cerradura in the southwestern EES. Such redox oscillations could also explain the high Mn/Al at some sites (e.g., Bodin et al., 2010; Rodríguez-Tovar & Reolid, 2013). Organic compounds derived from green sulfur bacteria have been found at some Italian sites in the southern EES (Pancost et al., 2004), possibly suggesting sporadic photic zone euxinia. We note that samples from the southern EES also vary in TOC content: sedimentary rocks from sites in Morocco, Italy, and Greece contain lower TOC (e.g., Bodin et al., 2010; Kafousia et al., 2014) than sites in Spain and Portugal.

4.3. Ocean Dynamics During the T-OAE

In our simulations, the main pattern of ocean circulation in the Tethys Ocean consists of a strong westward equatorial current that transports warm and salty waters to the southern EES (Figures 4a and 4c–4h). These waters are mostly flushed away from the epicontinental sea through the Hispanic Corridor to the Panthalassa Ocean, except if the connection is closed (Figure 4). The surface currents entering the EES slow down at the mouth of the Hispanic Corridor, but they keep a clockwise motion following the east and SW Laurasian coast. The shallow bathymetry, the numerous sills and islands in the northeastern EES also contribute to the weakening of these current. A shallowing of the EES bathymetry further slows down these northeast currents (Figure 4h). This gyre-like pattern dominates the EES in all scenarios, including in those performed with MITgcm (Figure 4h), and we refer to this circulation pattern as the large-scale Tethyan clockwise gyre.

The large-scale gyre is also present in coastal bottom waters (~100–300 m), which is especially visible in the $PR1_{InsolStrong}$ scenario (Figure 4b). The vertical profile of the E-W velocity component (*u*) in a transect at the boundary between the EES and the open Tethys Ocean mostly follows the surface dynamics (Figure 4a).

Note that the N-S velocity component (*v*) is close to zero along the reference transect at 27°E. Although the large-scale Tethyan clockwise gyre is present in all scenarios (including in those performed by Dera & Donnadieu, 2012), the ventilation and strength of the global ocean overturning is strongly affected by changes in initial sea surface temperatures, continental configuration and orbital forcing (supporting information Figure S2.2). For example, when assuming a weak insolation in the Northern Hemisphere, the ocean overturning is significantly reduced in the Northern Hemisphere relative to PR1 (with a difference of up to 10 Sv; Figure S2.2b).

Part of the equatorial surface waters entering the EES is transported back to the Tethys Ocean before reaching the shallowest eastern part of the EES (around 10–15°N). This is particularly the case when the Hispanic Corridor is narrow (PR2 and $PR2_{shallow}$; Figures 4f and 4g) or closed ($PR1_{closed}$; Figure 4e). The dimensions, strength, and position of this pattern, here referred to as the southern small-scale gyre, vary in scenarios with different bathymetry and orbital forcing. The pattern is not present in the scenarios performed with MITgcm (Figures 4h and 5a).

The salinity distribution and the vertical mixing show a clear difference between the northern and the southern EES in all runs, which is consistent with the large-scale Tethyan clockwise gyre described before. An example for $PR2_{MIT}$ is shown in Figure 5a, where the salinity in the southern EES remains close to the mean ocean value (~35). In contrast, the northern basins are significantly less saline than in the south (~33). Similarly, north of the 30°N parallel, the mixed layer depth is significantly shallower than in the southern EES, reaching 20 to 30 m *versus* 40 to 100 m, respectively (Figure 5b).

Changes in orbital forcing affect the flow in the Viking and Hispanic Corridors. Compared to our baseline scenario (PR1), the experiment with a weak seasonal contrast in the Northern Hemisphere ($PR1_{InsolWeak}$) is characterized by a more vigorous surface ocean circulation (Figure 6). More specifically, the surface small-scale gyre, the surface currents of the Viking Corridor (Figure 6a), and the currents flowing out of the EES to the open Tethys Ocean are enhanced (Figure 6b). However, the surface currents in the Hispanic Corridor (Figure 6a) and the E-W velocities of the coastal bottom waters entering the EES from the open Tethys Ocean (Figure 6c) are reduced. A shallowing of the EES, potentially reduces the ocean dynamics of the large-scale Tethyan gyre (Figure 4g).

4.4. Organic Carbon Burial

From the data compilation, we estimate an average TOC content across the T-OAE of 6.7 wt% and an average thickness of the deposit of 7 m (Table S1) for the anoxic northern basins. The anoxic area during the T-OAE is estimated at 1.2×10^6 km^2 (supporting information Figure S1.2), and the corresponding burial of organic carbon in the anoxic northern basins is then calculated at 1,104 Gt of carbon. The suboxic and the oxic areas of the EES are estimated at 2.5×10^6 and 2.7×10^6 km^2, which could have buried an additional 1,300 and 202 Gt of carbon, respectively. In this case the assumption is that the T-OAE deposits in the suboxic and oxic areas have TOC contents of 1.5 and 0.5 wt% and an average thickness of 14 and 6.2 m, respectively (supporting information Table S1).

5. Discussion

5.1. Temporal Variability in Oxygenation in the Northern EES

Various lines of evidence suggest that the northern basins were susceptible to low oxygen, for example, due to recurrent inputs of Arctic nutrient-rich seawater (Dera & Donnadieu, 2012), a bathymetry that favored restriction (McArthur et al., 2008), and climate conditions that promoted continental weathering (Cohen et al., 2004; Fantasia et al., 2018; Hesselbo et al., 2007) and enhanced precipitation along the western Laurasian coast (Chandler et al., 1992; Valdes et al., 1995). Nonetheless, the redox proxy records for Yorkshire, Dotternhausen, and Schandelah suggest that bottom waters in the northern EES were mainly oxic before the initiation of T-OAE (Figure 2). This is deduced from the low TOC/P ratios, near crustal average of Fe/Al, and the nearly constant background values of Mo, S, V, and Cu prior to the carbon isotope excursion associated with the T-OAE. Severe oxygen depletion occurred at the onset of the T-OAE, after which low-oxygen conditions persisted within the entire interval at all three sites. Our redox proxy and data compilation (Figures 2 and 3) shows that the anoxia was not limited to the southern German and Cleveland basins (Dickson et al., 2017; Fantasia et al., 2018; McArthur et al., 2008; Pearce et al., 2008; Them et al., 2018; Thibault et al., 2018) but is likely to have dominated the entire northeastern EES. Prolonged periods of photic zone euxinia are also likely to have

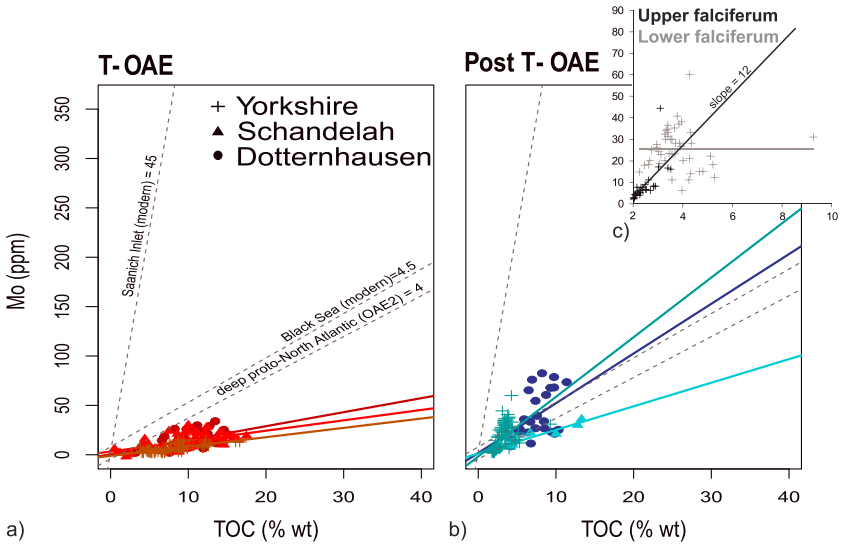

Figure 7. Crossplot of sediment Mo versus TOC for (a) the T-OAE interval and (b) after the termination of T-OAE at Dotternhausen (●), Schandelah (▲), and Yorkshire (+). Corresponding regression slopes are indicated with the same color as the symbol. Dashed lines show regression slopes for Mo and TOC data of the well mixed Saanich Inlet, the restricted modern Black Sea (Algeo & Lyons, 2006), and the restricted deep proto-North Atlantic during OAE2 (van Helmond et al., 2014). Specific regression lines for the (c) lower and upper *falciferum* Subzones in Yorkshire are plotted to show differences within the *falciferum* Subzone. TOC = total organic carbon; T-OAE = Toarcian Oceanic Anoxic Event.

occurred (Frimmel et al., 2004; Montero-Serrano et al., 2015; Pancost et al., 2004; Röhl & Schmid-Röhl, 2005; Schouten et al., 2000).

To assess the degree of restriction of the water column at our three sites during the T-OAE, crossplots of sediment TOC and Mo content were compared with TOC and Mo crossplots for modern sediments from the well-ventilated Saanich Inlet and the restricted Black Sea (Algeo & Lyons, 2006) and Cretaceous OAE2 sediments (van Helmond et al., 2014; Figure 7). We find that the regression lines for the T-OAE of our three sites plot below the regression lines for the Black Sea and OAE2 (Figure 7a), in accordance with results reported previously for Yorkshire (McArthur et al., 2008; Pearce et al., 2008; Them et al., 2018; Thibault et al., 2018), indicating extremely restricted conditions.

After the T-OAE (Figure 7b), most redox proxies show evidence for improved oxygenation, but not necessarily oxic conditions (e.g., Dickson et al., 2017; McArthur et al., 2008; Them et al., 2018; Thibault et al., 2018). The rise in Mo concentration in the lower *falciferum* Subzone after the T-OAE at all sites is likely due to a decrease in the area subject to euxinia and an increase in the Mo inventory (e.g., Dickson et al., 2017; McArthur et al., 2008; Pearce et al., 2008). However, the TOC, the Mo inventory, and the ocean dynamics in these basins necessarily varied within the *falciferum* Subzone. This is further illustrated by the differences between the regression lines between TOC and Mo for the upper and lower *falciferum* Subzone at Yorkshire (Figure 7c).

Brief oxygenation periods may have occurred in the EES during the T-OAE (Caswell & Coe, 2013, 2014; Montero-Serrano et al., 2015; Röhl et al., 2001; Röhl & Schmid-Röhl, 2005). In our records, this is especially visible from maxima in Fe/Al and Mn at the base of T-OAE at Schandelah and in the middle of the T-OAE at Dotternhausen (Figure 2). Fluctuations in the Mo isotope composition of T-OAE sedimentary rocks from the northeastern basins have been attributed to changes in the local hydrography and water exchange with the open ocean (Dickson et al., 2017). Short-lived oxygenation events may be linked to a switch from monsoon winds to dry northeast trade winds (Röhl et al., 2001) and/or to variations in the ocean circulation strength. Our numerical experiments suggest that the southward flow through the Viking Corridor could have been enhanced temporarily as the general ocean circulation changed (Figure 6). As a consequence cold-oxygenated waters could have been transported to the northeastern EES. Conversely, the intensification of anoxia may be linked to a weakening of the Arctic southward flow. However, because these particular oxygenation events are not recorded at all northeastern sites, they could also represent local changes rather than fluctuations in ocean dynamics. Alternatively, brief ventilation events may not have led to well-oxygenated bottom waters at all three sites due to differences in paleodepths (Röhl & Schmid-Röhl, 2005) and paleo-

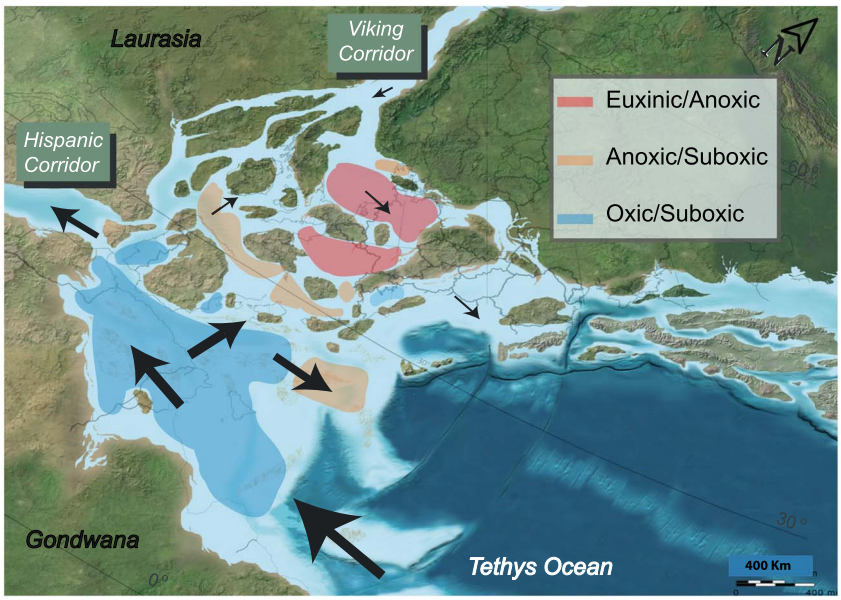

Figure 8. Dominant flow patterns as deduced from the ocean modeling and areas characterized by euxinic/anoxic, anoxic/suboxic, and oxic/suboxic bottom water conditions based on the geological compilation and modeling results.

geography, or these events might simply not have been captured in the sampling or preserved in the record. Changes in external forcing alter the position and current velocities of the clockwise gyre dominating the EES (Figures 4 and 6). This modulates the water and thus oxygen exchange between the EES and the Tethys Ocean. For example, changes in seasonal contrast in the Northern Hemisphere or a reduction in the pCO_2 (Dera & Donnadieu, 2012) facilitate ventilation in bottom waters of the southern EES (Figures 4, 6, and S2.2). Thus, orbital changes and a decrease in pCO_2 levels toward the termination of T-OAE could have worked synergistically to favor a vigorous ocean circulation that, together with cooling, led to a reduced hydrological cycle and thus reduced continental weathering. This is in agreement with the return to nearly zero kaolinite/illite ratios (Xu et al., 2018) and lower osmium isotope values (Cohen et al., 2004; Percival et al., 2016; Them et al., 2017) observed at the termination of the T-OAE. Although further studies on the temporal evolution of the ocean dynamics during the Toarcian are needed, this study suggests that major changes through time and geographically observed in the redox proxy records of the northern EES are likely to be linked to variations in the ocean circulation and to have contributed to the termination of T-OAE.

5.2. Spatial Trends in Bottom Water Oxygen and Ocean Dynamics in the EES

Our data compilation (Figure 3 and Table S1) indicates that there were distinct spatial differences in bottom water oxygen between the northern and southern EES. While the restricted basins along the northeastern coast of the EES were anoxic with periods of photic zone euxinia during T-OAE, the southern EES remained mostly oxygenated. Our modeling results confirm that ocean dynamics in the EES, notably the Tethyan large-scale clockwise gyre, permitted the development of two contrasting vertical mixing regimes on both sides of the 30°N parallel: a vigorous mixing regime in the southern sector and a sluggish regime in the restricted northern basins (Figure 5b). The weak circulation in the northern EES made this oceanic region highly sensitive to continental runoff and thus stratification. Independent paleobiogeographical studies also show this marked partitioning between the northern and the southern EES (with the boundary at ~30°N) with limited exchange of fauna during the Pliensbachian (e.g., Dera et al., 2011; Zacaï et al., 2016) that may have lasted until the initiation of T-OAE. We suggest that in addition to relative sea level rise, the redox gradient, together with ocean dynamics, created distinct ecological niches between the northern and the southern EES. A summary of the dominant spatial differences in bottom water redox conditions and key features of the prevailing circulation during the T-OAE deduced from the geological compilation and model results is shown in Figure 8.

The clockwise gyre over the northern Tethyan Ocean observed in all our simulations is a robust result that agrees with Toarcian paleoclimate reconstructions (Krencker et al., 2015; Röhl et al., 2001) and previous modeling studies (Dera & Donnadieu, 2012). The gyre is thought to have formed due to the continental configuration

and the Coriolis force that favored a surface circular motion and brought equatorial warm water masses towards the central EES (Krencker et al., 2015). The results from FOAM and MITgcm indicate that the clockwise gyre not only dominated the surface Tethys Ocean but also affected deeper waters (Figure 4b). We further suggest that most warm Tethys waters were flushed from the EES through the Hispanic Corridor. Thus, only weak northward currents reached the northwestern basins. This water motion does not support the hypothesis of a dominant pattern with Tethys waters reaching the Arctic region through the Viking Corridor proposed by Korte et al. (2015) based on $\delta^{18}O$. The discrepancy between both theories could be explained by a larger salinity effect on $\delta^{18}O$ than that assumed by Korte et al. (2015).

The strong westward limb of the large-scale gyre flowing from the open equatorial Tethys Ocean toward the southern EES likely oxygenated the waters along the North African coast (Figure 8). This implies that the equatorial open Tethys Ocean was oxygenated as well. In contrast, the sluggish northward limb of the gyre, the shallow bathymetry, the abundant sills, and islands did not allow easy flushing of preestablished anoxic bottom waters in the northern basins. Evidence from changes in the composition of microfossil and macrofossil assemblages suggest a gradual water stratification and the development of a stable pycnocline in the northern EES during the T-OAE (Bucefalo Palliani et al., 2002; Caswell & Coe, 2013), which further supports our modeling results for the northern EES (Figure 5). We suggest that in addition to the bathymetry and relative sea level change (Röhl et al., 2001), the northern basins were highly restricted due to weakening of the northward arm of the large-scale gyre in the NE Tethys region. In addition, our results suggest that a secondary small-scale southern gyre could have modified local nutrient conditions in the central EES (Figures 4 and 6), affecting sites such as Mochras, Sancerre, Creux de l'Ourse, Dogna, and Petousi (Figures 1, 3, and 8). However, during the Toarcian, orbital forcing and bathymetry were certainly not constant and, thus, temporal shifts between sluggish and vigorous ocean dynamics in the EES are possible. Such variations could have led to a waxing and waning of the anoxic area in the northeast and could explain the occasional occurrence of euxinia/anoxia at some southern sites (Pancost et al., 2004; Reolid et al., 2014).

The northeastern basins received riverine nutrient input from the Laurasian continent where wet conditions prevailed (Cohen et al., 2004; Dera & Donnadieu, 2012; Hesselbo et al., 2007; Valdes et al., 1995). The high nutrient supply likely contributed to elevated productivity at the northern sites (i.e., Yorkshire, Dotternhausen, Schandelah, Gipf, Riniken, and Rietheim; e.g., Cohen et al., 2004; Fantasia et al., 2018; Montero-Serrano et al., 2015). Both the enhanced primary productivity and the restricted nature of the basins favored the decline in bottom water oxygen concentrations. The high TOC/P ratios (Figure 3) indicate a strong recycling of P that may have further sustained primary productivity. Such recycling of P likely played a key role in the development of ocean anoxia during various periods of Earth history including Cretaceous OAEs and the PETM (Dickson et al., 2014; Kraal et al., 2010; Mort et al., 2007; Ruvalcaba Baroni et al., 2014; Tsandev & Slomp, 2009). In contrast, river input to the southern EES was likely to have been small during the T-OAE. This conclusion is based on the deposition of evaporites along the North African coast (Baudin et al., 1990; Gordon, 1975), which suggest very dry conditions and low terrigenous input at the coastal Amellago site (Figure 3; Bodin et al., 2010).

Overall, severe deoxygenation in the EES during the T-OAE was mostly confined to the northern basins (Figure 8), where the recovery after the T-OAE was relatively slow due to weak currents in this region (Figure 4). Thus, sluggish local water dynamics would not have allowed easy flushing of preestablished anoxic bottom waters and may explain the restriction that continued after T-OAE, despite a potential increase in the global ocean circulation strength.

5.3. Implications for Organic Carbon Burial

The Toarcian negative carbon isotope excursion can be explained by release of methane into the atmosphere from methane clathrates (21,000 Gt of carbon; Beerling & Berner, 2002) or thermogenic methane (31,000 Gt of carbon; Xu et al., 2017). Besides weathering of silicates, sequestration of carbon through burial in marine sediments may be a major driver behind the recovery from the negative carbon isotope excursion (Jenkyns, 2010).

Recently, Xu et al. (2017) suggested that the freshwater paleo-Sichuan lake (with an area of 230,000 km^2) accounted for burial of 460 Gt of carbon or 1.3% to 2.2% of the total carbon drawdown required for the T-OAE recovery. Based on our model bathymetry and data compilation (Figures 3 and S1.2), we estimate that the anoxic/euxinic northern basins of the EES accounted for about 0.3% of the area of the global ocean, and, at 1,104 Gt of carbon, buried ~2.4 times more carbon than the lake. The amount of carbon sequestered from the atmosphere by the euxinic northern basins alone during the T-OAE black-shale deposition thus repre-

sents about 3.2% to 5.3% of the total carbon required for the recovery of the negative $\delta^{13}C$ excursion. When considering that the other areas in the EES also were characterized by an increased burial of organic carbon, assuming a total area of 5.2×10^6 km^2 (i.e., the suboxic plus the oxic area), there is an additional burial of ~1,660 Gt of carbon. This suggests that the entire EES, which represents less than 3% of the Toarcian global ocean surface, could have accounted for up to 12% of the carbon burial required to explain the carbon isotope recovery. In addition, other coastal basins with high organic carbon burial may have existed elsewhere on Earth, as published sections are currently geographically limited. However, several sites with high organic carbon during the T-OAE have been found in, for example, the Neuquén Basin and Yakon River (Argentina; Al-Suwaidi et al., 2010, 2016), Haida Gwaii (British Columbia, Canada; Caruthers et al., 2011), and Toyora (Japan; Kemp & Izumi, 2014). In addition, other anoxic basins in which sediments are no longer preserved may have developed during the T-OAE. We conclude that the EES, together with other marine coastal areas, is likely to have acted as a key sink for atmospheric carbon during the Toarcian.

Interestingly, the area of anoxic waters estimated for the Cretaceous OAE2 is an order of magnitude larger than that calculated here for the EES and was mainly confined to the proto-North Atlantic (Dickson et al., 2016; Owens et al., 2013). The burial of organic carbon, which was most pronounced on the continental shelves (e.g., Nederbragt et al., 2004; van Bentum et al., 2009), has been suggested to have played a key role in removing carbon from the atmosphere during OAE2 (Barclay et al., 2010; Graly et al., 2017). The continental shelves of the proto–North Atlantic during OAE2 accounted for about 1.5% of the total ocean surface area (estimated from Ruvalcaba Baroni et al., 2014; Topper et al., 2011). This, together with our estimates of organic carbon burial in the EES, indicates that biogeochemical processes in a relatively small area of the ocean can impact the global carbon cycle and thus climate.

6. Conclusion

This study summarizes redox proxy data for the waters over the EES during the T-OAE and uses ocean circulation modeling to explain the observed spatial trends. We demonstrate that bottom water anoxia/euxinia was most pronounced in the restricted basins along the northeastern coast, while bottom waters on the southwestern shelf were mostly oxic or suboxic during the event. Our model results indicate that the ocean circulation in the Tethyan region was characterized by a clockwise gyre, which played a key role in controlling the oxygen distribution in the EES. The oxygenated bottom waters on the southwestern shelf can be attributed to the less restricted nature of this region and input of well oxygenated waters from the adjacent Tethys Ocean. Because of more sluggish circulation in the northeastern regions, these areas were not well ventilated and anoxia and euxinia developed. High ratios of TOC/P indicate strong recycling of phosphorus relative to organic carbon. This recycling may have helped sustain a high productivity and the anoxia in the northeastern basins. Organic carbon burial in the EES may have been responsible for removal of up to 12% of the total carbon required to explain the observed recovery of the global carbon isotope excursion. This supports the hypothesis that a small coastal area, such as the EES, which accounts for about 3% of the surface ocean, can impact the global carbon cycle through burial of organic carbon. Organic carbon burial in the EES is likely to have played a key role in the recovery from the Toarcian Oceanic Anoxic Event.

Acknowledgments
This research was funded by the Netherlands Earth System Science Center (NESSC), financially supported by the Ministry of Education, Culture and Science (OCW), the European Research Council under the European Community's Seventh Framework Programme (FP7/ 2007/20072013)/ERC Starting Grant 278364, the Netherlands Organisation for Scientific Research (NWO; Vici grant 865.13.005), and the Natural Environment Research Council, UK (studentship to Harding). We thank Arnold van Dijk, Carolien van der Weijst, Helen de Waard, and Ton Zalm for analytical assistance. We thank Ton Markus for support with the illustrations. We thank Tanya Goldberg for sharing unpublished organic carbon data for site F11-01. Climate modeling was supported by the CEA/CCRT who provided access to the HPC resources of TGCC (allocation 2014-012212 by GENCI). We also thank Poulsen, Algeo, and an anonymous reviewer for carefully reading our manuscript and for their constructive comments. New data for this study are available at Ruvalcaba et al. (2018): PANGAEA, https://doi.pangaea/10.1594/.

References

Aberhan, M. (2001). Bivalve palaeobiogeography and the Hispanic Corridor: Time of opening and effectiveness of a proto-Atlantic seaway. *Palaeogeography, Palaeoclimatology, Palaeoecology*, *165*(3), 375–394.

Aberhan, M. (2002). Opening of the Hispanic Corridor and Early Jurassic bivalve biodiversity. *Geological Society, London, Special Publications*, *194*(1), 127–139.

Adcroft, A., Hill, C., Campin, J.-M., Marshall, J., & Heimbach, P. (2004). Overview of the formulation and numerics of the MIT GCM. In *Proceedings of the ECMWF seminar series on Numerical Methods, Recent developments in numerical methods for atmosphere and ocean modelling* (pp. 139–149). Reading, UK.

Al-Suwaidi, A., Angelozzi, G., Baudin, F., Damborenea, S., Hesselbo, S., Jenkyns, H., et al. (2010). First record of the Early Toarcian Oceanic Anoxic Event from the Southern Hemisphere, Neuquén Basin, Argentina. *Journal of the Geological Society*, *167*(4), 633–636.

Al-Suwaidi, A. H., Hesselbo, S. P., Damborenea, S. E., Manceñido, M. O., Jenkyns, H. C., Riccardi, A. C., et al. (2016). The Toarcian Oceanic Anoxic Event (Early Jurassic) in the Neuquén Basin, Argentina: A reassessment of age and carbon isotope stratigraphy. *The Journal of Geology*, *124*(2), 171–193.

Algeo, T. J., & Ingall, E. (2007). Sedimentary C_{org}: P ratios, paleocean ventilation, and Phanerozoic atmospheric pO_2. *Palaeogeography Palaeoclimatology Palaeoecology*, *256*, 130–155.

Algeo, T. J., & Lyons, T. W. (2006). Mo–total organic carbon covariation in modern anoxic marine environments: Implications for analysis of paleoredox and paleohydrographic conditions. *Paleoceanography and Paleoclimate*, *21*(1), PA1016.

Algeo, T. J., & Maynard, J. B. (2004). Trace–element behavior and redox facies in core shales of Upper Pennsylvanian Kansas-type cyclothems. *Chemical geology*, *206*(3), 289–318.

Arias, C. (2006). Northern and Southern Hemispheres ostracod palaeobiogeography during the Early Jurassic: Possible migration routes. *Palaeogeography, Palaeoclimatology, Palaeoecology*, *233*(1), 63–95.

Barclay, R. S., McElwain, J. C., & Sageman, B. B. (2010). Carbon sequestration activated by a volcanic CO_2 pulse during Ocean Anoxic Event 2. *Nature Geoscience*, *3*(3), 205.

Baudin, F., Herbin, J.-P., Bassoullet, J.-P., Dercourt, J., Lachkar, G., Manivit, H., & Renard, M. (1990). Distribution of organic matter during the Toarcian in the Mediterranean Tethys and Middle East. *Deposition of organic facies. Association of American Petroleum Geologists, Studies in Geology*, *30*, 73–92.

Beerling, D., & Berner, R. (2002). Biogeochemical constraints on the Triassic-Jurassic boundary carbon cycle event. *Global Biogeochemical Cycles*, *16*(3), 1036.

Berner, R. A. (1970). Sedimentary pyrite formation. *American journal of science*, *268*(1), 1–23.

Bjerrum, C. J., Surlyk, F., Callomon, J. H., & Slingerland, R. L. (2001). Numerical paleoceanographic study of the Early Jurassic transcontinental Laurasian Seaway. *Paleoceanography and Paleoclimate*, *16*(4), 390–404.

Bodin, S., Mattioli, E., Fröhlich, S., Marshall, J., Boutib, L., Lahsini, S., & Redfern, J. (2010). Toarcian carbon isotope shifts and nutrient changes from the Northern margin of Gondwana (High Atlas, Morocco, Jurassic): Palaeoenvironmental implications. *Palaeogeography, Palaeoclimatology, Palaeoecology*, *297*(2), 377–390.

Boulila, S., Galbrun, B., Huret, E., Hinnov, L. A., Rouget, I., Gardin, S., & Bartolini, A. (2014). Astronomical calibration of the Toarcian Stage: Implications for sequence stratigraphy and duration of the early Toarcian OAE. *Earth and Planetary Science Letters*, *386*, 98–111.

Brumsack, H.-J. (1991). Inorganic geochemistry of the German Posidonia Shale: Palaeoenvironmental consequences. *Geological Society, London, Special Publications*, *58*(1), 353–362.

Bucefalo Palliani, R., Mattioli, E., & Riding, J. B. (2002). The response of marine phytoplankton and sedimentary organic matter to the early Toarcian (Lower Jurassic) Oceanic Anoxic Event in northern England. *Marine Micropaleontology*, *46*(3), 223–245.

Calvert, S., & Pedersen, T. (1996). Sedimentary geochemistry of manganese: Implications for the environment of formation of manganiferous black shales. *Economic Geology*, *91*(1), 36–47.

Caruthers, A. H., Gröcke, D. R., & Smith, P. L. (2011). The significance of an Early Jurassic (Toarcian) carbon-isotope excursion in Haida Gwaii (Queen Charlotte Islands), British Columbia, Canada. *Earth and Planetary Science Letters*, *307*(1-2), 19–26.

Caswell, B. A., & Coe, A. L. (2013). Primary productivity controls on opportunistic bivalves during Early Jurassic oceanic deoxygenation. *Geology*, *41*(11), 1163–1166.

Caswell, B. A., & Coe, A. L. (2014). The impact of anoxia on pelagic macrofauna during the Toarcian Oceanic Anoxic Event (Early Jurassic). *Proceedings of the Geologists' Association*, *125*(4), 383–391.

Chandler, M. A., Rind, D., & Ruedy, R. (1992). Pangaean climate during the Early Jurassic: GCM simulations and the sedimentary record of paleoclimate. *Geological Society of America Bulletin*, *104*(5), 543–559.

Cochlan, W., Harrison, P., & Denman, K. (1991). Diel periodicity of nitrogen uptake by marine phytoplankton in nitrate-rich environments. *Limnology and Oceanography*, *36*(8), 1689–1700.

Cohen, A. S., Coe, A. L., Harding, S. M., & Schwark, L. (2004). Osmium isotope evidence for the regulation of atmospheric O_2 by continental weathering. *Geology*, *32*(2), 157–160.

Cohen, A. S., Coe, A. L., & Kemp, D. B. (2007). The Late Palaeocene–Early Eocene and Toarcian (Early Jurassic) carbon isotope excursions: A comparison of their time scales, associated environmental changes, causes and consequences. *Journal of the Geological Society, London*, *164*(6), 1093–1108.

Dera, G., & Donnadieu, Y. (2012). Modeling evidences for global warming, Arctic seawater freshening, and sluggish oceanic circulation during the Early Toarcian anoxic event. *Paleoceanography and Paleoclimate*, *27*(2), PA2211.

Dera, G., Neige, P., Dommergues, J.-L., & Brayard, A. (2011). Ammonite paleobiogeography during the Pliensbachian–Toarcian crisis (Early Jurassic) reflecting paleoclimate, eustasy, and extinctions. *Global and Planetary Change*, *78*(3), 92–105.

Dera, G., Prunier, J., Smith, P. L., Haggart, J. W., Popov, E., Guzhov, A., et al. (2015). Nd isotope constraints on ocean circulation, paleoclimate, and continental drainage during the Jurassic breakup of Pangea. *Gondwana Research*, *27*(4), 1599–1615.

Dera, G., Pucéat, E., Pellenard, P., Neige, P., Delsate, D., Joachimski, M. M., et al. (2009). Water mass exchange and variations in seawater temperature in the NW Tethys during the Early Jurassic: Evidence from neodymium and oxygen isotopes of fish teeth and belemnites. *Earth and Planetary Science Letters*, *286*(1), 198–207.

Dickson, A. J., Gill, B. C., Ruhl, M., Jenkyns, H. C., Porcelli, D., Idiz, E., et al. (2017). Molybdenum-isotope chemostratigraphy and paleoceanography of the Toarcian Oceanic Anoxic Event (Early Jurassic). *Paleoceanography and Paleoclimate*, *32*, 813–829.

Dickson, A. J., Jenkyns, H. C., Porcelli, D., van den Boorn, S., & Idiz, E. (2016). Basin-scale controls on the molybdenum-isotope composition of seawater during Oceanic Anoxic Event 2 (Late Cretaceous). *Geochimica et Cosmochimica Acta*, *178*, 291–306.

Dickson, A. J., Rees-Owen, R. L., März, C., Coe, A. L., Cohen, A. S., Pancost, R. D., et al. (2014). The spread of marine anoxia on the northern Tethys margin during the Paleocene-Eocene Thermal Maximum. *Paleoceanography and Paleoclimatology*, *29*(6), 471–488.

Eckert, S., Brumsack, H.-J., Severmann, S., Schnetger, B., März, C., & Fröllje, H. (2013). Establishment of euxinic conditions in the Holocene Black Sea. *Geology*, *41*(4), 431–434.

Falcón, L. I., Carpenter, E. J., Cipriano, F., Bergman, B., & Capone, D. G. (2004). N_2 fixation by unicellular bacterioplankton from the Atlantic and Pacific Oceans: Phylogeny and in situ rates. *Applied and environmental microbiology*, *70*(2), 765–770.

Fantasia, A., Föllmi, K. B., Adatte, T., Spangenberg, J. E., & Montero-Serrano, J.-C. (2018). The Early Toarcian Oceanic Anoxic Event: Paleoenvironmental and paleoclimatic change across the Alpine Tethys (Switzerland). *Global and Planetary Change*, *162*, 53–68.

Farrow, G. E. (1966). Bathymetric zonation of Jurassic trace fossils from the coast of Yorkshire, England. *Palaeogeography, Palaeoclimatology, Palaeoecology*, *2*, 103–151.

Ferreira, D., Marshall, J., & Rose, B. (2011). Climate determinism revisited: Multiple equilibria in a complex climate model. *Journal of Climate*, *24*(4), 992–1012.

Forget, G., Campin, J., Heimbach, P., Hill, C., Ponte, R., & Wunsch, C. (2015). ECCO version 4: An integrated framework for non-linear inverse modeling and global ocean state estimation. *Geoscientific Model Development*, *8*(10), 3071.

French, K. L., Sepulveda, J., Trabucho-Alexandre, J., Gröcke, D., & Summons, R. E. (2014). Organic geochemistry of the early Toarcian Oceanic Anoxic Event in Hawsker Bottoms, Yorkshire, England. *Earth and Planetary Science Letters*, *390*, 116–127.

Frimmel, A., Oschmann, W., & Schwark, L. (2004). Chemostratigraphy of the Posidonia Black Shale, SW Germany: I. Influence of sea-level variation on organic facies evolution. *Chemical Geology*, *206*(3), 199–230.

Gent, P. R., & Mcwilliams, J. C. (1990). Isopycnal mixing in ocean circulation models. *Journal of Physical Oceanography*, *20*(1), 150–155.

Golonka, J., & Ford, D. (2000). Pangean (late Carboniferous–Middle Jurassic) paleoenvironment and lithofacies. *Palaeogeography, Palaeoclimatology, Palaeoecology*, *161*(1), 1–34.

Gordon, W. A. (1975). Distribution by latitude of Phanerozoic evaporite deposits. *The Journal of Geology*, *83*(6), 671–684.

Gough, D. (1981). Solar interior structure and luminosity variations. In *Physics of Solar Variations* (pp. 21–34). Springer.
Graly, J. A., Drever, J. I., & Humphrey, N. F. (2017). Calculating the balance between atmospheric CO_2 drawdown and organic carbon oxidation in subglacial hydrochemical systems. *Global Biogeochemical Cycles*, *31*(4), 709–727.
Harding, S. M. (2004). The Toarcian Oceanic Anoxic Event: Organic and inorganic geochemical anomalies in organic-carbon-rich mudrocks from the North Yorkshire coast, UK and Dotternhausen Quarry, SW Germany (Doctoral dissertation). The Open University, UK.
Hastings, D. W., Emerson, S. R., & Mix, A. C. (1996). Vanadium in foraminiferal calcite as a tracer for changes in the areal extent of reducing sediments. *Paleoceanography and Paleoclimate*, *11*(6), 665–678.
Helz, G., Miller, C., Charnock, J., Mosselmans, J., Pattrick, R., Garner, C., & Vaughan, D. (1996). Mechanism of molybdenum removal from the sea and its concentration in black shales: EXAFS evidence. *Geochimica et Cosmochimica Acta*, *60*(19), 3631–3642.
Hermoso, M., Le Callonnec, L., Minoletti, F., Renard, M., & Hesselbo, S. P. (2009). Expression of the Early Toarcian negative carbon-isotope excursion in separated carbonate microfractions (Jurassic, Paris Basin). *Earth and Planetary Science Letters*, *277*(1), 194–203.
Hesselbo, S. P., Gröcke, D. R., Jenkyns, H. C., Bjerrum, C. J., Farrimond, P., Bell, H. S. M., & Green, O. R. (2000). Massive dissociation of gas hydrate during a Jurassic Oceanic Anoxic Event. *Nature*, *406*(6794), 392–395.
Hesselbo, S. P., Jenkyns, H. C., Duarte, L. V., & Oliveira, L. C. (2007). Carbon-isotope record of the Early Jurassic (Toarcian) Oceanic Anoxic Event from fossil wood and marine carbonate (Lusitanian Basin, Portugal). *Earth and Planetary Science Letters*, *253*(3), 455–470.
Howarth, M. K. (1992). The Ammonite family Hildoceratidae in the Lower Jurassic of Britain. *Palaeontographical Society Monograph, London*, 590, 1–200.
Huang, C., & Hesselbo, S. P. (2014). Pacing of the Toarcian Oceanic Anoxic Event (Early Jurassic) from astronomical correlation of marine sections. *Gondwana Research*, *25*(4), 1348–1356.
Ingall, E. D., Bustin, R. M., & Van Cappellen, P. (1993). Influence of water column anoxia on the burial and preservation of carbon and phosphorus in marine shales. *Geochimica et Cosmochimica Acta*, *57*, 303–316.
Jacob, R. L. (1997). Low frequency variability in a simulated atmosphere ocean system (Ph.D. thesis), University of Wisconsin–Madison.
Jacob, R., Schafer, C., Foster, I., Tobis, M., & Anderson, J. (2001). Computational design and performance of the Fast Ocean Atmosphere Model, version one. *Computational Science ICCS 2001*, *2073*, 175–184.
Jenkyns, H. C. (1985). The Early Toarcian and Cenomanian-Turonian anoxic events in Europe: Comparisons and contrasts. *Geologische Rundschau*, *74*(3), 505–518.
Jenkyns, H. C. (1988). The early Toarcian (Jurassic) anoxic event—Stratigraphic, sedimentary, and geochemical evidence. *American Journal of Science*, *288*(2), 101–151.
Jenkyns, H. C. (2010). Geochemistry of oceanic anoxic events. *Geochemistry Geophyics Geosystems*, *11*(3), 1–30.
Jenkyns, H. C., Gröcke, D. R., & Hesselbo, S. P. (2001). Nitrogen isotope evidence for water mass denitrification during the early Toarcian (Jurassic) Oceanic Anoxic Event. *Paleoceanography and Paleoclimate*, *16*(6), 593–603.
Jenkyns, H. C., Jones, C. E., GrÖcke, D. R., Hesselbo, S. P., & Parkinson, D. N. (2002). Chemostratigraphy of the Jurassic System: Applications, limitations and implications for palaeoceanography. *Journal of the Geological Society*, *159*(4), 351–378.
Kafousia, N., Karakitsios, V., Mattioli, E., Kenjo, S., & Jenkyns, H. (2014). The toarcian Oceanic Anoxic Event in the Ionian zone, Greece. *Palaeogeography, Palaeoclimatology, Palaeoecology*, *393*, 135–145.
Kemp, D. B., Coe, A. L., Cohen, A. S., & Schwark, L. (2005). Astronomical pacing of methane release in the Early Jurassic period. *Nature*, *437*(7057), 396–399.
Kemp, D. B., Coe, A. L., Cohen, A. S., & Weedon, G. P. (2011). Astronomical forcing and chronology of the early Toarcian (Early Jurassic) Oceanic Anoxic Event in Yorkshire, UK. *Paleoceanography*, *26*, PA4210. https://doi.org/10.1029/2011PA002122
Kemp, D. B., & Izumi, K. (2014). Multiproxy geochemical analysis of a Panthalassic margin record of the early Toarcian Oceanic Anoxic Event (Toyora area, Japan). *Palaeogeography, Palaeoclimatology, Palaeoecology*, *414*, 332–341.
Korte, C., Hesselbo, S. P., Ullmann, C. V., Dietl, G., Ruhl, M., Schweigert, G., & Thibault, N. (2015). Jurassic climate mode governed by ocean gateway. *Nature communications*, *6*(10), 015.
Kraal, P., Slomp, C. P., Forster, A., & Kuypers, M. M. M. (2010). Phosphorus cycling from the margin to abyssal depths in the proto-Atlantic during Oceanic Anoxic Event 2. *Palaeogeography Palaeoclimatology Palaeoecology*, *295*, 42–54.
Krencker, F.-N., Bodin, S., Suan, G., Heimhofer, U., Kabiri, L., & Immenhauser, A. (2015). Toarcian extreme warmth led to tropical cyclone intensification. *Earth and Planetary Science Letters*, *425*, 120–130.
Large, W. G., McWilliams, J. C., & Doney, S. C. (1994). Oceanic vertical mixing: A review and a model with a nonlocal boundary layer parameterization. *Reviews of Geophysics*, *32*(4), 363–403.
Lenz, C., Jilbert, T., Conley, D., Wolthers, M., & Slomp, C. (2015). Are recent changes in sediment manganese sequestration in the euxinic basins of the Baltic Sea linked to the expansion of hypoxia? *Biogeosciences*, *12*(16), 4875–4894.
Lu, Z., Jenkyns, H. C., & Rickaby, R. E. (2010). Iodine to calcium ratios in marine carbonate as a paleo-redox proxy during Oceanic Anoxic Events. *Geology*, *38*(12), 1107–1110.
Lyons, T. W., Anbar, A. D., Severmann, S., Scott, C., & Gill, B. C. (2009). Tracking euxinia in the ancient ocean: A multiproxy perspective and Proterozoic case study. *Annual Review of Earth and Planetary Sciences*, *37*, 507–534.
Lyons, T. W., & Berner, R. A. (1992). Carbon-sulfur-iron systematics of the uppermost deep-water sediments of the Black Sea. *Chemical Geology*, *99*(1-3), 1–27.
Lyons, T. W., & Severmann, S. (2006). A critical look at iron paleoredox proxies: New insights from modern euxinic marine basins. *Geochimica et Cosmochimica Acta*, *70*(23), 5698–5722.
Mailliot, S., Mattioli, E., Bartolini, A., Baudin, F., Pittet, B., & Guex, J. (2009). Late Pliensbachian–Early Toarcian (Early Jurassic) environmental changes in an epicontinental basin of NW Europe (Causses area, central France): A micropaleontological and geochemical approach. *Palaeogeography, Palaeoclimatology, Palaeoecology*, *273*(3), 346–364.
Marshall, J., Jones, H., & Hill, C. (1998). Efficient ocean modeling using non-hydrostatic algorithms. *Journal of Marine systems*, *18*(1), 115–134.
Mattioli, E., Pittet, B., Suan, G., & Mailliot, S. (2008). Calcareous nannoplankton changes across the early Toarcian Oceanic Anoxic Event in the western Tethys. *Paleoceanography and Paleoclimate*, *23*(3), PA3208.
McArthur, J., Algeo, T., Van de Schootbrugge, B., Li, Q., & Howarth, R. (2008). Basinal restriction, black shales, Re-Os dating, and the Early Toarcian (Jurassic) Oceanic Anoxic Event. *Paleoceanography and Paleoclimate*, *23*(4), PA4217.
McElwain, J. C., Wade-Murphy, J., & Hesselbo, S. P. (2005). Changes in carbon dioxide during an Oceanic Anoxic Event linked to intrusion into Gondwana coals. *Nature*, *435*(7041), 479.
Montero-Serrano, J.-C., Föllmi, K. B., Adatte, T., Spangenberg, J. E., Tribovillard, N., Fantasia, A., & Suan, G. (2015). Continental weathering and redox conditions during the early Toarcian Oceanic Anoxic Event in the northwestern Tethys: Insight from the Posidonia Shale section in the Swiss Jura Mountains. *Palaeogeography, Palaeoclimatology, Palaeoecology*, *429*, 83–99.

Mort, H. P., Adatte, T., Föllmi, K. B., Keller, G., Steinmann, P., Matera, V., et al. (2007). Phosphorus and the roles of productivity and nutrient recycling during Oceanic Anoxic Event 2. *Geology*, *35*, 483–486.
Mort, H. P., Slomp, C. P., Gustafsson, B. G., & Andersen, T. J. (2010). Phosphorus recycling and burial in Baltic Sea sediments with contrasting redox conditions. *Geochimica et Cosmochimca Acta*, *74*, 1350–1362.
Nederbragt, A. J., Thurow, J., Vonhof, H., & Brumsack, H.-J. (2004). Modelling oceanic carbon and phosphorus fluxes: Implications for the cause of the late Cenomanian Oceanic Anoxic Event (OAE2). *Journal of the Geological Society of London*, *161*(4), 721–728.
Nikitenko, B. (2008). The Early Jurassic to Aalenian paleobiogeography of the Arctic Realm: Implication of microbenthos (Foraminifers and Ostracodes). *Stratigraphy and Geological correlation*, *16*(1), 59–80.
Owens, J. D., Gill, B. C., Jenkyns, H. C., Bates, S. M., Severmann, S., Kuypers, M. M., et al. (2013). Sulfur isotopes track the global extent and dynamics of euxinia during Cretaceous Oceanic Anoxic Event 2. *Proceedings of the National Academy of Sciences*, *110*(46), 18,407–18,412.
Owens, J. D., Lyons, T. W., Li, X., Macleod, K. G., Gordon, G., Kuypers, M. M. M., et al. (2012). Iron isotope and trace metal records of iron cycling in the proto-North Atlantic during the Cenomanian-Turonian Oceanic Anoxic Event (OAE-2). *Palaeogeography*, *27*, 1–13.
Pacanowski, R., & Philander, S. (1981). Parameterization of vertical mixing in numerical models of tropical oceans. *Journal of Physical Oceanography*, *11*(11), 1443–1451.
Pancost, R. D., Crawford, N., Magness, S., Turner, A., Jenkyns, H. C., & Maxwell, J. R. (2004). Further evidence for the development of photic-zone euxinic conditions during Mesozoic Oceanic Anoxic Events. *Journal of the Geological Society of London*, *161*(3), 353–364.
Parrish, J. T., & Curtis, R. L. (1982). Atmospheric circulation, upwelling, and organic rich rocks in the Mesozoic and Cenozoic eras. *Palaeogeography Palaeoclimatology Palaeoecology*, *40*, 31–66.
Pearce, C. R., Cohen, A. S., Coe, A. L., & Burton, K. W. (2008). Molybdenum isotope evidence for global ocean anoxia coupled with perturbations to the carbon cycle during the Early Jurassic. *Geology*, *36*(3), 231–234.
Percival, L. M., Cohen, A., Davies, M., Dickson, A., Hesselbo, S., Jenkyns, H., et al. (2016). Osmium isotope evidence for two pulses of increased continental weathering linked to Early Jurassic volcanism and climate change. *Geology*, *44*(9), 759–762.
Pohl, A., Donnadieu, Y., Le Hir, G., & Ferreira, D. (2017). The climatic significance of Late Ordovician-early Silurian black shales. *Paleoceanography and Paleoclimate*, *32*(4), 397–423.
Raiswell, R., & Anderson, T. (2005). Reactive iron enrichment in sediments deposited beneath euxinic bottom waters: Constraints on supply by shelf recycling. *Geological Society, London, Special Publications*, *248*(1), 179–194.
Reolid, M., Emanuela, M., Nieto, L. M., & Rodríguez-Tovar, F. J. (2014). The Early Toarcian Oceanic Anoxic Event in the External Subbetic (Southiberian Palaeomargin, Westernmost Tethys): Geochemistry, nannofossils and ichnology. *Palaeogeography, Palaeoclimatology, Palaeoecology*, *411*, 79–94.
Riegraf, W., Werner, G., & Lörcher, F. (1984). Der Posidonienschiefer: Biostratigraphie, Fauna und Fazies des südwestdeutschen Untertoarciums (Lias e). F. Enke.
Rodríguez-Tovar, F. J., & Reolid, M. (2013). Environmental conditions during the Toarcian Oceanic Anoxic Event (T–OAE) in the westernmost Tethys: Influence of the regional context on a global phenomenon. *Bulletin of Geosciences*, *88*(4), 697–712.
Röhl, H.-J., & Schmid-Röhl, A. (2005). Lower Toarcian (Upper Liassic) black shales of the Central European epicontinental basin: A sequence stratigraphic case study from the SW German Posidonia Shale.
Röhl, H.-J., Schmid-Röhl, A., Oschmann, W., Frimmel, A., & Schwark, L. (2001). The Posidonia Shale (Lower Toarcian) of SW-Germany: An oxygen-depleted ecosystem controlled by sea level and palaeoclimate. *Palaeogeography, Palaeoclimatology, Palaeoecology*, *165*(1), 27–52.
Ruebsam, W., Müenzberger, P., & Schwark, L. (2014). Chronology of the Early Toarcian environmental crisis in the Lorraine Sub-Basin (NE Paris Basin). *Earth and Planetary Science Letters*, *404*, 273–282.
Ruvalcaba Baroni, I., Coe, A. L., Harding, S. M., Papadomanolaki, N. M, van Helmond, N. A. G. M., van de Schootbrugge, B., et al. (2018). Biogeochemical redox proxies in sediments from Yorkshire (UK), Schandelah (N Germany) and Dotternhausen (S Germany) during the Toarcian (Early Jurassic). PANGAEA. https://doi.pangaea.de/10.1594/PANGAEA.892961
Ruvalcaba Baroni, I., Topper, R. P. M., van Helmond, N. A. G. M., Brinkhuis, H., & Slomp, C. P. (2014). Biogeochemistry of the North Atlantic during Oceanic Anoxic Event 2: Role of changes in ocean circulation and phosphorus input. *Biogeosciences*, *11*(4), 977–993.
Schouten, S., van Kaam-Peters, H. M., Rijpstra, W. I. C., Schoell, M., & Damste, J. S. S. (2000). Effects of an Oceanic Anoxic Event on the stable carbon isotopic composition of early Toarcian carbon. *American Journal of Science*, *300*(1), 1–22.
Scott, C., & Lyons, T. W. (2012). Contrasting molybdenum cycling and isotopic properties in euxinic versus non-euxinic sediments and sedimentary rocks: Refining the paleoproxies. *Chemical Geology*, *324*, 19–27.
Sellwood, B. W., & Valdes, P. J. (2008). Jurassic climates. *Proceedings of the Geologists' Association*, *119*(1), 5–17.
Sha, J., Olsen, P. E., Pan, Y., Xu, D., Wang, Y., Zhang, X., et al. (2015). Triassic–Jurassic climate in continental high-latitude Asia was dominated by obliquity-paced variations (Junggar Basin, Ürümqi, China). *Proceedings of the National Academy of Sciences*, *112*(12), 3624–3629.
Silva, R. L., Carlisle, C. M., & Wach, G. (2017). A new TOC, Rock-Eval, and carbon isotope record of Lower Jurassic source rocks from the Slyne Basin, offshore Ireland. *Marine and Petroleum Geology*, *86*, 499–511.
Slomp, C. P., Thomson, J., & de Lange, G. J. (2002). Enhanced regeneration of phosphorus during formation of the most recent eastern Mediterranean sapropel (S1). *Geochimica et Cosmochimica Acta*, *66*, 1171–1184.
Suan, G., Mattioli, E., Pittet, B., Mailliot, S., & Lécuyer, C. (2008). Evidence for major environmental perturbation prior to and during the Toarcian (Early Jurassic) Oceanic Anoxic Event from the Lusitanian Basin, Portugal. *Paleoceanography and Paleoclimate*, *23*(1), PA1202.
Suan, G., Pittet, B., Bour, I., Mattioli, E., Duarte, L. V., & Mailliot, S. (2008). Duration of the Early Toarcian carbon isotope excursion deduced from spectral analysis: Consequence for its possible causes. *Earth and Planetary Science Letters*, *267*(3-4), 666–679.
Sulu-Gambari, F., Roepert, A., Jilbert, T., Hagens, M., Meysman, F. J., & Slomp, C. P. (2017). Molybdenum dynamics in sediments of a seasonally-hypoxic coastal marine basin. *Chemical Geology*, *466*, 627–640.
Svensen, H., Planke, S., Chevallier, L., Malthe-Sørenssen, A., Corfu, F., & Jamtveit, B. (2007). Hydrothermal venting of greenhouse gases triggering Early Jurassic global warming. *Earth and Planetary Science Letters*, *256*(3-4), 554–566.
Them, T. R., Gill, B. C., Caruthers, A. H., Gerhardt, A. M., Gröcke, D. R., Lyons, T. W., et al. (2018). Thallium isotopes reveal protracted anoxia during the Toarcian (Early Jurassic) associated with volcanism, carbon burial, and mass extinction. *Proceedings of the National Academy of Sciences*. https:doi.org/10.1073/pnas.1803478115
Them, T. R., Gill, B. C., Selby, D., Gröcke, D. R., Friedman, R. M., & Owens, J. D. (2017). Evidence for rapid weathering response to climatic warming during the Toarcian Oceanic Anoxic Event. *Scientific Reports*, *7*(1), 5003.
Thibault, N., Ruhl, M., Ullmann, C. V., Korte, C., Kemp, D. B., Gröcke, D. R., & Hesselbo, S. P. (2018). The wider context of the Lower Jurassic Toarcian Oceanic Anoxic Event in Yorkshire coastal outcrops, UK. *Proceedings of the Geologists' Association*, *129*(3), 372–391.
Tissot, B., Califet-Debyser, Y., Deroo, G., & Oudin, J. (1971). Origin and evolution of hydrocarbons in early Toarcian shales, Paris Basin, France. *AAPG Bulletin*, *55*(12), 2177–2193.

Tobis, M., Schafer, C., Foster, I., Jacob, R., & Anderson, J. (1997). Foam: Expanding the horizons of climate modeling. In *Proceedings of the 1997 ACM/IEEE conference on Supercomputing* (pp. 1–15). San Jose, CA: ACM.

Topper, R. P. M., Trabucho Alexandre, J., Tuenter, E., & Meijer, TH. P. (2011). A regional ocean circulation model for the mid-Cretaceous North Atlantic Basin: Implications for black shale formation. *Climate of the past*, *7*, 277–297.

Trabucho-Alexandre, J., Dirkx, R., Veld, H., Klaver, G., & de Boer, P. L. (2012). Toarcian black shales in the Dutch Central Graben: Record of energetic, variable depositional conditions during an Oceanic Anoxic Event. *Journal of sedimentary Research*, *82*(2), 104–120.

Tribovillard, N., Algeo, T. J., Lyons, T., & Riboulleau, A. (2006). Trace metals as paleoredox and paleoproductivity proxies: An update. *Chemical geology*, *232*(1), 12–32.

Tsandev, I., & Slomp, C. P. (2009). Modeling phosphorus cycling and carbon burial during Cretaceous Oceanic Anoxic Events. *Earth and Planetary Science Letters*, *286*(1), 71–79.

Valdes, P., Sellwood, B., & Price, G. (1995). Modelling late Jurassic Milankovitch climate variations. *Geological Society, London, Special Publications*, *85*(1), 115–132.

van Bentum, E. C., Hetzel, A., Brumsack, H.-J., Forster, A., Reichart, G.-J., & Sinninghe Damsté, J. S. (2009). Reconstruction of water column anoxia in the equatorial Atlantic during the Cenomanian-Turonian Oceanic Anoxic Event using biomarker and trace metal proxies. *Palaeogeography Palaeoclimatology Palaeoecology*, *280*, 489–498.

Van Breugel, Y., Baas, M., Schouten, S., Mattioli, E., & Sinninghe Damsté, J. S. (2006). Isorenieratane record in black shales from the Paris Basin, France: Constraints on recycling of respired CO_2 as a mechanism for negative carbon isotope shifts during the Toarcian Oceanic Anoxic Event. *Paleoceanography and Paleoclimate*, *21*(4), 1–8.

van Eldijk, T. J., Wappler, T., Strother, P. K., van der Weijst, C. M., Rajaei, H., Visscher, H., & van de Schootbrugge, B. (2018). A Triassic–Jurassic window into the evolution of Lepidoptera. *Science advances*, *4*(1), e1701568.

van Helmond, N. A., Ruvalcaba Baroni, I., Sluijs, A., Sinninghe Damsté, J. S., & Slomp, C. P. (2014). Spatial extent and degree of oxygen depletion in the deep proto-North Atlantic basin during Oceanic Anoxic Event 2. *Geochemistry, Geophysics, Geosystems*, *15*(11), 4254–4266.

Van Santvoort, P. J. M., De Lange, G., Thomson, J., Colley, S., Meysman, F., & Slomp, C. (2002). Oxidation and origin of organic matter in surficial Eastern Mediterranean hemipelagic sediments. *Aquatic Geochemistry*, *8*(3), 153–175.

van de Schootbrugge, B., Bachan, A., Suan, G., Richoz, S., & Payne, J. L. (2013). Microbes, mud and methane: Cause and consequence of recurrent Early Jurassic anoxia following the end-Triassic mass extinction. *Palaeontology*, *56*(4), 685–709.

van de Schootbrugge, B., McArthur, J. M., Bailey, T., Rosenthal, Y., Wright, J., & Miller, K. (2005). Toarcian Oceanic Anoxic Event: An assessment of global causes using belemnite C isotope records. *Paleoceanography and Paleoclimate*, *20*(3), PA3008.

van de Schootbrugge, B., Richoz, S., Pross, J., Luppold, F., Hunze, S., Wonik, T., et al. (2018). The Schandelah Scientific Drilling Project: A 25-million year record of Early Jurassic palaeo-environmental change from northern Germany. Accepted for publication, Newsletters on Stratigraphy.

Wei, L., Mastalerz, M., Schimmelmann, A., & Chen, Y. (2014). Influence of Soxhlet-extractable bitumen and oil on porosity in thermally maturing organic-rich shales. *International Journal of Coal Geology*, *132*, 38–50.

Wignall, P. B., Newton, R. J., & Little, C. T. (2005). The timing of paleoenvironmental change and cause-and-effect relationships during the Early Jurassic mass extinction in Europe. *American Journal of Science*, *305*(10), 1014–1032.

Xu, W., Ruhl, M., Jenkyns, H. C., Hesselbo, S. P., Riding, J. B., Selby, D., et al. (2017). Carbon sequestration in an expanded lake system during the Toarcian Oceanic Anoxic Event. *Nature Geoscience*, *10*(2), 129–134.

Xu, W., Ruhl, M., Jenkyns, H. C., Leng, M. J., Huggett, J. M., Minisini, D., et al. (2018). Evolution of the Toarcian (Early Jurassic) carbon-cycle and global climatic controls on local sedimentary processes (Cardigan Bay Basin, UK). *Earth and Planetary Science Letters*, *484*, 396–411.

Zacaï, A., Brayard, A., Dommergues, J.-L., Meister, C., Escarguel, G., Laffont, R., et al. (2016). Gauging scale effects and biogeographical signals in similarity distance decay analyses: An Early Jurassic ammonite case study. *Palaeontology*, *59*(5), 671–687.

Ziegler, P. A. (1988). Evolution of the Arctic-North Atlantic and the Western Tethys: A visual presentation of a series of Paleogeographic-Paleotectonic maps. *AAPG memoir*, *43*, 164–196.

Ziegler, P. A. (1990). Geological atlas of western and central Europe. Geological Society of London.